The effects of small water surfaces on turbulent flow in the atmospheric boundary layer URANS approach implemented in OpenFOAM

Abbasi, Ali; Annor, Frank Ohene; van de Giesen, Nick

DOI
10.1016/j.envsoft.2017.12.013

Publication date
2018

Document Version
Final published version

Published in
Environmental Modelling & Software

Environmental Modelling & Software 101 (2018) 268–288

Contents lists available at ScienceDirect

Environmental Modelling & Software

journal homepage: www.elsevier.com/locate/envsoft

The effects of small water surfaces on turbulent flow in the atmospheric boundary layer: URANS approach implemented in OpenFOAM

Ali Abbasi [a, b, *], Frank Ohene Annor [b, c], Nick van de Giesen [b]

[a] Department of Civil Engineering, Faculty of Engineering, Ferdowsi University of Mashhad, Mashhad, Iran
[b] Department of Water Resources, Faculty of Civil Engineering and Geosciences, Delft University of Technology, Stevinweg 1, 2628 CN, Delft, The Netherlands
[c] Civil Engineering Department, Kwame Nkrumah University of Science and Technology, Kumasi, Ghana

ARTICLE INFO

Article history:
Received 16 June 2016
Received in revised form
18 December 2017
Accepted 20 December 2017
Available online 10 January 2018

Keywords:
Small water surface
ABL
Stability condition
Roughness lengths
OpenFOAM
URANS

ABSTRACT

A 3-D numerical method is developed to investigate the spatial distribution of surface fluxes over heterogeneous surfaces in (semi-)arid regions. Quantifying the effects of changes in the momentum, thermal and moisture roughness lengths on the airflow and fluxes in the ABL is important for water resources management and local climate studies. The governing equations and turbulence models are modified to include the effects of atmospheric stability conditions on the airflow. The turbulent airflow in ABL is simulated based on the Unsteady Reynolds-Averaged Navier-Stokes (URANS) approach to understand the air flow over the non-homogeneous surfaces from dry land through the water surface and vice versa. The model can be used to study airflow in neutral and non-neutral ABL over complex and non-homogeneous surfaces. The model results were used to investigate the flow parameters and (heat) flux variations over small water surfaces considering its surrounding conditions.

1. Introduction

In regional hydrological cycles, small water bodies represent a significant part of the water budget. However, in most of the current mesoscale and global atmospheric models, the influences of small inland water bodies in the surface parametrization are neglected (Swayne et al., 2005). The most important issue of inland water bodies is the lake-atmosphere exchange process which should be considered through water surface fluxes such as momentum, heat convection and evaporation of water (Vercauteren, 2011). In comparison to land surfaces, inland water surfaces such as small lakes and reservoirs have different interactions with the atmospheric boundary layer above them with regards to evaporation, wind speed and heat exchanges over the water surfaces (Swayne et al., 2005). However, implementing these effects in Atmospheric Boundary Layer (ABL) models introduces extra complexities in its simulations, especially in regions with huge numbers of small water surfaces. One complexity of the water-atmosphere interaction in regional climate model comes from the fact that the presence of lakes has significant effects on the atmosphere dynamics due to the change of roughness length, moisture contents and temperature of water versus that of land (Beniston, 1986). The distribution of the sensible and latent heat fluxes can affect the flow on small, regional and global scales, where the exchanges of water vapor, heat and momentum over grid cells should be improved for water surface (Giorgi and Avissar, 1997; Avissar and Pielkea, 1989; Gao et al., 2008; Lyons and Halldin, 2004; Pielke and Uliasz, 1998; Wu et al., 2009).

Understanding and modeling the correlation of the atmospheric boundary layer with its underlying water surface is crucial for a wide range of scientific research such as developing inland water surface evaporation models, atmosphere simulations, and investigating climate change influences on inland water bodies (Edson et al., 2007; Parlange et al., 1995). Due to the logistical difficulties and economic issues in operating measurements over water surfaces, especially for small reservoirs, water-atmosphere interaction has been studied less than land-atmosphere interaction (DeCosmo et al., 1996; Heikinheimo et al., 1999; Sun et al., 2001; Vickers and

* Corresponding author. Department of Civil Engineering, Faculty of Engineering, Ferdowsi University of Mashhad, Mashhad, Iran.
E-mail addresses: aabbasi@um.ac.ir (A. Abbasi), annorfrank@yahoo.co.uk (F.O. Annor), n.c.vandegiesen@tudelft.nl (N. van de Giesen).

https://doi.org/10.1016/j.envsoft.2017.12.013
1364-8152/

Mahrt, 2010).

The effect of roughness changes on the atmospheric boundary layer flow has been studied extensively by several researchers, especially in micro-meteorology. Some of these research examined the air flow and flux exchange in ABL by using theoretical analyses (e.g. Bradley (1968); Jackson (1976); Petersen and Taylor (1973); Raupach et al. (1980, 1996)) and some of them used field measurements or wind tunnel studies (e.g. Cao and Tamura (2006); Nadeau et al. (2011); Rider et al. (1964); Dyer and Crawford (1965); Davenport and Hudson (1967); Lang et al. (1974, 1983); Lettau and Zabransky (1968); Panofsky and Townsend (1964); Panofsky and Petersen (1972); Petersen and Taylor (1973); Munro and Oke (1975); Figuerola and Berliner (2005)) to understand the problem of sharp changes in the roughness length. However, measurements of spatial variations in the ABL are challenging and require the use of several pieces of equipment (Mahrt et al., 1994). Most of these research mainly focused on momentum and heat exchange above land.

Previous research works investigated airflow over heterogeneous surfaces such as complex terrains and rural and urban type environments which consist of different surfaces. Vercauteren (2011) investigated the lake-atmosphere process by using the Lake-Atmosphere Turbulent EXchange (LATEX) field measurement over Lake Geneva. Pendergrass and Arya (1984) simulated the effects of sharp roughness changes of rural and urban type surfaces on the development of the Internal Boundary Layer (IBL) under a neutral condition. Fesquet et al. (2009) investigated the influences of different atmospheric stability conditions and fetch effects on ABL turbulent airflow over heterogeneous terrains. They showed that the local turbulence variables such as momentum fluxes are significantly affected by the land surface complexity (Fesquet et al., 2009). By using a three-dimensional Large Eddy Simulation (LES) model, Fesquet et al. (2009) studied the effects of surface inhomogeneities on the ABL flow structure.

A big challenge in simulations of atmospheric boundary layer over heterogeneous surfaces (for instance a surface consists of land and water surface) is that there are sharp changes of the surfaces properties from land to water surface and vice versa. In addition, small inland water bodies usually have a limited fetch and dependent on the fetch values, the airflow over the lakes has time or not to adjust to its underlying water surface. In these cases, the horizontal inhomogeneity can be very important and the effect of this limited fetch still needs to be assessed (Vercauteren, 2011; Brutsaert, 1982). Such strong spatial differences in surface characteristics (temperature, wetness and the roughness) affect the airflow and transfer processes of heat and water vapor, specifically the evaporation rates. In response to these changes, an internal boundary layer develops that characterizes the region influenced by the wet surface.

Following rapid changes in surface properties from land to water or vice versa downwind of a step change location, an Internal Boundary Layer (IBL) develops which is strongly dependent on the surface below. In this situation, only the lowest parts of the atmosphere may be affected by the underlying surface conditions and the flow structure in higher levels is usually mainly dependent on the upwind surface conditions (Pendergrass and Arya, 1984).

Measuring airflow parameters over the water surface usually is costly and time consuming. Hence, due to the lack of measurements over the water surface, especially for small and shallow lakes (which are rarely available or usually confined to a single point), modeling the atmospheric boundary layer (ABL) flow would be promising for spatial information of air flow passing over different surfaces. Computational Fluid Dynamics (CFD) simulations help to understand the interactions of inland water bodies with the surrounding atmosphere. CFD as a robust tool can provide the temporal and spatial distribution of airflow parameters in the computational domain, which is difficult to achieve using experimental measurements, to investigate the effects of the water surfaces on the above atmosphere.

The atmospheric boundary layer flow is usually turbulent and fully developed. Studying the turbulent flow in ABL alongside the size of atmospheric domains is an ongoing challenge to simulate realistic atmospheric flows. To simulate the turbulent flow dynamics in the lower atmosphere, the Reynolds-Averaged Navier-Stokes (RANS) approach has been widely utilized (e.g. Solazzo et al. (2009); Majdoubi et al. (2009); Milashuk and Crane (2011); Anagnostopoulos and Bergeles (1998); Foudhil et al. (2005); Pattanapol et al. (2008); Luna et al. (2003); Liu et al. (1996); Prospathopoulos et al. (2012); Hsieh et al. (2007); Huser et al. (1997)). Although recently due to the significant growth in computing tools and consequently a decrease in simulation cost, more accurate methods with more computational needs, such as Large Eddy Simulation (LES) is becoming more applicable in ABL studies (e.g. Benjamin et al. (2011); Flores et al. (2013); Beyers et al. (2010); Hertwig et al. (2011); Chamecki et al. (2008); Albertson and Parlange (1999); Porté-Agel et al. (2014); Cancelli et al. (2014); Porté-Agel et al. (2011); Maronga et al. (2013); Esau and Lyons (2002); Bou-Zeid (2004); Vercauteren et al. (2008)). The water surface and land fluxes of momentum, heat and water vapor determine the state of the atmosphere to a large extent. Their accurate parametrization has been recognized as a big challenge to make CFD a more reliable tool for simulation of airflow over heterogeneous surfaces which include small water surfaces (Cabot and Moin, 1999; Piomelli and Balaras, 2002; Piomelli, 2008). A review of numerical studies of flow over wet surfaces can be found for example in Crosman and Horel (2010).

Considering the dimensions of the computational domain, the global and mesoscale models of atmospheric flow are not applicable to study the small waters effects on airflow because of the hydrostatic pressure assumption and their inabilities in resolving the variations in topography in vertical direction and consequently roughness variations in the simulation (Kim et al., 2000). Fully 2-D and 3-D atmosphere models can be used to provide reliable predictions considering various conditions to investigate the airflow in the ABL. Although, adding the third dimension to the model usually makes the model more complex and expensive due to the high computational requirements, these three-dimensional models provide accurate airflow predictions over the complex terrain which is not possible with one- or two-dimensional simulations (Joubert et al., 2012).

In the present research, the state of the airflow in the atmosphere as it passes from a dry land surface to a wet (water) surface is considered. The effect of a surface transition and sharp changes in surfaces properties (such as roughness length, wetness and temperature) on the flow are investigated. In addition, the atmospheric stability conditions are considered in the simulation to study the effect of stability conditions on the airflow over a non-homogeneous surface. The RANS approach is used to study the airflow and heat fluxes above a small inland water surface surrounded by arid lands.

2. Model structure

In atmospheric boundary layer (ABL), the flow is represented by the conservation laws of mass, momentum and energy. Combining the airflow and heat transfer in the ABL introduces extra complexities to the simulation. Even though the thermodynamic properties of air are assumed to be constant, the buoyancy body force term in the momentum equation is added allowing one to relate density changes to temperature in ABL. In the model

developed in this study, it is assumed that the ABL airflow is incompressible and fully three-dimensional.

The RANS approach has been applied to simulate the ABL flow due to its computational feasibility Although using other approaches such as Direct Numerical Simulation (DNS) or Large Eddy Simulation (LES) methods would generate more precise results, they are not applicable in most of ABL airflow modeling because applying these approaches for real-life complex geometries needs a very fine computational grid and consequently high computational resources (Wakes et al., 2010). Based on the turbulence model used, the numerical scheme, and the discretization technique, wide range of RANS models with different complexity levels have been developed in ABL modeling. In using the RANS approach to resolve the turbulence of the airflow, some (zero, one, two or even more) additional equations must be solved alongside the flow equations (Prospathopoulos et al., 2012; Tsanis et al., 2006; Tritton, 2007).

The different phases of the ABL modeling framework developed in this study are illustrated in Fig. 1.

2.1. Governing equations

The Navier-Stokes equations, as a widely used approach, are solved to model the airflow, heat (temperature) and water vapor (specific humidity) transfer over an inland water surface and its surrounding lands. With the assumption of the pressure work being negligible, the following conservation equations can be derived for mass, momentum and energy respectively (Defraeye et al., 2012; Ferziger and Perić, 2002; White, 1991; Massel, 1999; Zhang et al., 2005):

$$\frac{\partial u_i}{\partial x_i} = 0 \tag{1}$$

$$\frac{\partial u_i}{\partial t} + \frac{\partial}{\partial x_j}(u_j u_i) - \frac{\partial}{\partial x_j}\left\{\nu_{eff}\left[\left(\frac{\partial u_i}{\partial x_j} + \frac{\partial u_j}{\partial x_i}\right) - \frac{2}{3}\left(\frac{\partial u_k}{\partial x_k}\right)\delta_{ij}\right]\right\} = -\frac{1}{\rho_k}\frac{\partial p}{\partial x_i} + g_i\left[1 - \beta\left(T - T_{ref}\right)\right] \tag{2}$$

$$\frac{\partial T}{\partial t} + \frac{\partial}{\partial x_i}(T u_i) - \alpha_{eff}\frac{\partial}{\partial x_k}\left(\frac{\partial T}{\partial x_k}\right) = 0 \tag{3}$$

$$\frac{\partial q}{\partial t} + \frac{\partial}{\partial x_i}(q u_i) - \chi_{eff}\frac{\partial}{\partial x_k}\left(\frac{\partial q}{\partial x_k}\right) = 0 \tag{4}$$

where u_i is the velocity component in x_i direction (ms^{-1}), p is pressure (Pa), T is temperature (K), q is specific humidity ($g\ kg^{-1}$), $\nu_{eff} = \nu_0 + \nu_t$ is the effective kinematic viscosity ($m^2 s^{-1}$), with ν_0 and ν_t denoting molecular and turbulent viscosity, respectively, g_i the gravity acceleration components (ms^{-2}), T_{ref} reference temperature ($= 293.15K$), β the coefficient of expansion with temperature of the air ($Jkg^{-1}K^{-1}$) and δ is the delta of Kronecker (dimensionless), $\alpha_{eff} = \alpha_0 + \alpha_t$ is effective heat transfer conductivity ($m^2 s^{-1}$), with α_0 and α_t denoting molecular and turbulent thermal conductivity of air, respectively, ρ_k is the effective (driving) kinematic density (dimensionless) and χ_{eff} effective water vapor transfer coefficient (in this study it is assumed that $\chi_{eff} = \alpha_{eff}$). The

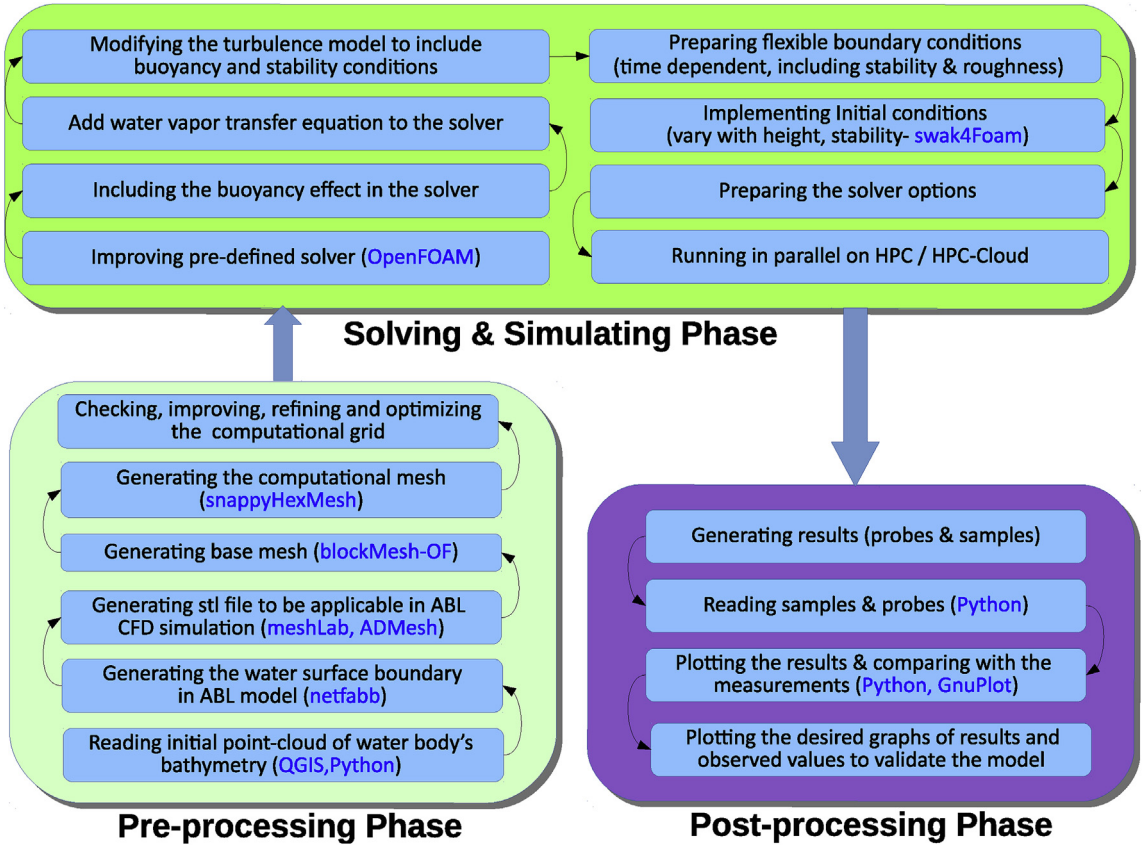

Fig. 1. Components of the ABL simulation framework developed in this study.

Boussinesq approximation is valid under the assumption that density differences are sufficiently small (as this study) to be neglected, except where they appear in the term multiplied by g_i (Fredriksson, 2011; Corzo et al., 2011). According to White (1991) and Ferziger and Perić (2002), the Boussinesq approximation introduces errors less than 1% for temperature variations of 15 K for air. In the model developed here, for incompressible flows the density of air is calculated as a linear function of temperature changes as

$$\rho = \rho_k \times \rho_0 \tag{5}$$

$$\rho_k = 1 - \beta\left(T - T_{ref}\right) \tag{6}$$

$$\beta = -\left(\frac{1}{\rho_0}\right)\frac{\partial \rho}{\partial T} \tag{7}$$

In the current model, a constant value for β (it is assumed air is an ideal gas) is used. Heat transfer conductivity in atmosphere can be given by:

$$\alpha_{eff} = \alpha_t + \alpha_0 = \frac{\nu_t}{Pr_t} + \frac{\nu_0}{Pr} \tag{8}$$

where Pr_t is turbulent Prandtl number and Pr is Prandtl number.

2.2. Turbulence model formulation

In ABL simulation, turbulence is not negligible and plays an important role (Crasto, 2007). Different turbulence models have been developed and applied in ABL simulations. The turbulence closures are applied in order to solve the Reynolds stresses and the scalar transport terms in the RANS approach. Investigation of different turbulence models used in RANS is beyond the aim of this study and comprehensive study of turbulence models can be found in Computational Fluid Dynamics books (e.g. Cebeci (2004); White (1991); Ferziger and Perić (2002), etc.).

Standard $k-\varepsilon$ (SKE) and realizable $k-\varepsilon$ (RKE) models are used widely in most CFD simulations. These turbulence approaches due to the relatively low computational needs, are considered as promising turbulence models in a wide-range of applications (Silvester et al., 2009). The semi-empirical standard model introduces two more transport equations for the turbulence kinetic energy (k) and the dissipation rate of kinetic energy (ε) in the flow equation system. Kim et al. (1997) and Kim and Patel (2000) showed that in comparison with other two-equation turbulence models, the $k-\varepsilon$ model requires less computational resources and can solve the airflow in ABL without loss of accuracy. Various two equation models (such as $k-\omega$) similar to the standard $k-\varepsilon$ model are available which need extra input parameters. In these models, the transport equation for k is derived mathematically while ε is based upon empirical definition (Silvester et al., 2009). According to Silvester et al. (2009), the standard $k-\varepsilon$ performs poorly for flows with steep pressure gradients and in cases with complex flows. The poor performance of $k-\varepsilon$ model mainly relates to imprecision in the ε equation (Hussein and El-Shishiny, 2009). However, the standard $k-\varepsilon$ model is mostly used for atmospheric boundary layer models. In simulating airflow alongside heat transfer in the regional atmosphere, it was found that the realizable $k-\varepsilon$ model is robust with reasonable accuracy and provides better results than the standard or other traditional $k-\varepsilon$ models (Shih et al., 1995; Wang, 2013; Joubert et al., 2012). In this turbulence model, the Reynolds stresses are limited by physical-based mathematical constraints (Rohdin and Moshfegh, 2007). In the RKE turbulence model, fluctuation of the dissipation rate is approximated by the dynamic equation of vorticity. In addition, the RKE is expected to accurately predict the flow variables and likely to enhance the stability of employed numerical schemes in ABL turbulent flow simulations (Shih et al., 1995). In the RKE model, the turbulence kinetic energy (k) and the turbulent dissipation rate (ε) are obtained from:

$$\frac{\partial k}{\partial t} + \frac{\partial}{\partial x_j}\left(k\, u_j\right) = \frac{\partial}{\partial x_j}\left[\left(\frac{\nu_t}{\sigma_k}\right)\frac{\partial k}{\partial x_j}\right] + \nu_T\left(\frac{\partial u_i}{\partial x_j} + \frac{\partial u_j}{\partial x_i}\right)\frac{\partial u_i}{\partial x_j} - \varepsilon + G_k + G_b \tag{9}$$

$$\frac{\partial \varepsilon}{\partial t} + \frac{\partial}{\partial x_j}\left(\varepsilon\, u_j\right) = \frac{\partial}{\partial x_j}\left(\frac{\nu_t}{\sigma_\varepsilon}\frac{\partial \varepsilon}{\partial x_j}\right) + C_1 S\varepsilon - C_{\varepsilon 2}\frac{\varepsilon^2}{k + \sqrt{\nu\varepsilon}} + C_{\varepsilon 1}C_{\varepsilon 3}\frac{\varepsilon}{k}G_b \tag{10}$$

where k is the turbulence kinetic energy, ε is the dissipation rate of turbulence kinetic energy, ν_0 and ν_t are molecular and turbulent viscosity respectively, G_b is the production of turbulent kinetic energy by the buoyancy, and G_k is the production of turbulent kinetic energy by the mean velocity gradient. The parameter $C_{\varepsilon 3}$ is the ratio of the velocity functions in the vertical and longitudinal directions and is not constant but instead depends on the flow conditions (Lee, 2007):

$$C_{\varepsilon 3} = \tanh\left|\frac{w}{U_h}\right| \tag{11}$$

where U_h and w are the components of the airflow velocity perpendicular and parallel to the gravitational vector, respectively. The coefficient C_1 is evaluated as (Shih et al., 1995):

$$C_1 = max\left(0.43, \frac{\zeta}{\zeta + 5}\right) \tag{12}$$

$$\zeta = S\,\frac{k}{\varepsilon} \tag{13}$$

$$S = \sqrt{2S_{ij}S_{ij}} \tag{14}$$

$$S_{ij} = \frac{1}{2}\left(\frac{\partial u_i}{\partial x_j} + \frac{\partial u_j}{\partial x_i}\right) \tag{15}$$

and the turbulent kinematic viscosity is given by

$$\nu_t = C_\mu \frac{k^2}{\varepsilon} \tag{16}$$

$$C_\mu = \frac{1}{A_0 + A_s\frac{kU^*}{\varepsilon}} \tag{17}$$

$$U^* = \sqrt{S_{ij}S_{ij} + \overline{\Omega_{ij}}\,\overline{\Omega_{ij}}} \tag{18}$$

$$A_s = \sqrt{6}\cos\phi \tag{19}$$

$$\phi = \frac{1}{3}cos^{-1}\left(\sqrt{6}\,W\right) \tag{20}$$

$$W = \frac{S_{ij}S_{jk}S_{ki}}{\tilde{S}^3} \tag{21}$$

$$\tilde{S} = \sqrt{S_{ij}S_{ij}} \tag{22}$$

$\overline{\Omega_{ij}}$ represents the mean rate-of-rotation tensor to capture rotational effects on the flow field. The production of turbulent kinetic energy by the mean velocity gradient (G_k) is written as:

$$G_k = \nu_t S^2 \tag{23}$$

In the current ABL airflow modeling, due to the existence of temperature gradient alongside the non-zero gravity field, the production of turbulent kinetic energy by the buoyancy is included in the k and ε equations (G_b in Equation (9) and Equation (10)). The generation of turbulence due to buoyancy is given by

$$G_b = \beta g_i \frac{\nu_t}{Pr_t}\left[\left(\frac{\partial T}{\partial x_i} - \frac{g_i}{C_p}\right)\right] \tag{24}$$

where Pr_t is the turbulent Prandtl number (a dimensionless number defined as the ratio of momentum diffusivity to thermal diffusivity which controls the relative thickness of the momentum and thermal boundary layers). For standard and realizable $k-\varepsilon$ models, default value of Pr_t for air is 0.71 (Fluent Manual, 2006). g_i is gravitational vector components, C_p is specific heat of air and T is (air) temperature. In unstable atmospheric conditions $G_b > 0$ and according to k equation (Equation (9))) the turbulence kinetic energy tends to be increased. In contrast to the unstable conditions, for stable stratification in ABL where $G_b < 0$, buoyancy force disrupts the turbulence intensity. To investigate the influence of atmospheric stability conditions on the airflow in ABL, the buoyancy terms in the k and ε should be used in turbulence model. While the process of generation of turbulence due to buoyancy on turbulent kinetic energy (k) is relatively clear, the effect of buoyancy on the dissipation rate of kinetic energy (ε) is less understood (Fluent Manual, 2006). In the current model, the buoyancy effects on both k and ε are included in turbulence model given by Equation (24). To take into account the buoyancy effects on ε, the non-constant parameter $C_{\varepsilon 3}$ is used as defined in Equation (11).

Exploring a wide-range of turbulent flow experiments (e.g. Shih et al. (1995) and Pieterse (2013)), values of the model constants of the realizable turbulence approach in the Equation (9) and Equation (10) are:

$$C_{\varepsilon 1} = 1.176; \quad C_{\varepsilon 2} = 1.92; \quad \sigma_k = 1.0; \quad \sigma_\varepsilon = 1.3; \quad A_0 = 4.0 \tag{25}$$

2.3. Atmospheric stability condition

The turbulent airflow in ABL is strongly influenced by the atmospheric stability conditions (Garratt, 1994). Some attempts have been made to take into consideration stability effects in simulating turbulent ABL (Alinot and Masson, 2005; Huser et al., 1997; Meissner et al., 2009; Pontiggia et al., 2009). In non-neutral conditions, the applied turbulence model should account for both shear and buoyancy produced turbulence terms. To consider the effects of atmospheric stability conditions in the ABL flow, the conservation of energy (or temperature), is included in the governing equations and coupled with the momentum equation. The buoyancy forces are taken into consideration using the Boussinesq approximation for buoyancy, and density variations are introduced only into the gravity terms of the momentum equations (Alinot and Masson, 2005; Meissner et al., 2009; Pontiggia et al., 2009). Additionally to buoyancy forces, thermal stratification in ABL has a significant impact on the turbulence characteristics. Therefore, the turbulence model has to be modified to take into account the generation and destruction of turbulence due to buoyancy. This is typically done via buoyancy term in k and ε equations. For determining the buoyancy related terms in turbulence equations different approaches exist in literature, and their formulations differ greatly (Huser et al., 1997; Sogachev et al., 2012; Vendel et al., 2010).

Generally, two different approaches can be applied for the consideration of atmospheric stability conditions in ABL simulations. In the first approach, the stability conditions are implemented in the vertical profiles of temperature and other parameters at the inflow boundary (free stream stability approach). To prepare these vertical profiles at the inflow, the stability conditions should be prescribed. This method is applied in Section (5). In the second approach, the stability conditions are implemented in time and location varying surface (skin) temperature or time-dependent non-uniform heat fluxes on the surface (surface stability approach) (Koblitz et al., 2015). In comparison with heat fluxes, using (measured) temperature values on the surfaces is more straightforward and introduces less uncertainties in the simulations. Due to the transient nature of ABL flow, in both approaches the boundary conditions used at the inflow and bottom boundaries are unsteady and vary with height and time (Section (4)). In the current study, the second approach has been used for lake Binaba (Section (6)) with the measured time varying surface temperatures for both land and water surfaces to reduce the uncertainties due to the heat fluxes calculations over the bottom boundary. More details about using heat fluxes as bottom boundary conditions can be found in Abbasi et al. (2017a).

2.4. Solver specifications

Steady-state solvers have been applied in many ABL simulation cases to predict the mean flow characteristics (Prospathopoulos et al., 2012). However, in some cases such as for the current study, the steady flow assumption is not strictly valid and would create large errors in the simulations, even in the micro-scale. Abrupt changes in the surface characteristics, time-dependent meteorological parameters, combining heat transfer with wind flow simulation, and unsteady (transient) boundary conditions especially over the water surface make it necessary to develop an unsteady solver to estimate flow parameters in this study.

The solver developed in this study solves the governing equations in the model described in Section (2.1) alongside the turbulence model equations described in Section (2.2) using boundary and initial conditions as described in Section (4.1). The ABL airflow equations are discretized using the Finite Volume Method (FVM) in open-source code OpenFOAM. The OpenFOAM (Open Source Field Operation and Manipulation) toolbox includes open source C++ libraries released under the general public license (GPL). Using pre-configured built-in libraries, one can build his own numerical solvers for solving the desired ABL airflow problems (Chen et al., 2014). The pre-configured solvers were modified and used for the current study. Considering the buoyancy effects in turbulence equations is an example of modification in the standard available solvers and libraries.

Furthermore, and unlike most commercial codes now available (e.g. ANSYS FLUENT, FIDAP, PHOENICS, STAR-CD, etc.), the pre-configured solvers and utilities in OpenFOAM could be extended to generate strictly customized tools and boundary conditions (BC). As OpenFOAM is available free and open-source, it will be a promising tool for research due to its adaptability to specific case

studies. In addition, in contrast to the commercial CFD packages, using OpenFOAM does not need any expensive licenses neither for commercial nor academic purposes (Benjamin et al., 2011). The free availability of this open source CFD software alongside its robustness could be a very attractive motivation to use it in developing countries (Balogh et al., 2012).

The OpenFOAM-based incompressible solver developed in the current context computes the airflow variables in the atmospheric boundary layer over a non-homogeneous surface. The presented solver has been built on the built-in solver in OpenFOAM called buoyantBoussinesqPimpleFoam, and some corrections, improvements and additions have been done to adapt it to the specific case study. This unsteady finite volume solver was used in this study to simulate airflow and heat transfer in the atmospheric boundary layer.

2.4.1. Solving algorithm

One of the main advantages of OpenFOAM is that it allows one to employ desired specific solver for each of the governing equations. From the results of some similar simulations done, throughout this work, the Euler blended Crank-Nicholson method was used to discretize the temporal term. This is a first-order, bounded implicit method and the Smooth Solver for the momentum, k, ε, T and q equations is used with a GaussSeidel smoother (Gauss refers to the standard finite volume discretization of Gaussian integration). The GAMG (Geometric-algebraic multi-grid) solver is used to solve the pressure equation. Multi-grid solvers (such as GAMG) decrease the computational time and show appropriate performance in problems of airflow over complex terrains. This solver is specially convenient and fast in highly dense domains. It first generates a quick solution on a coarser mesh (with a small number of cells) and then maps the resolved field data onto a finer mesh to obtain an accurate solution. With respect to the spatial discretization, gradient terms were solved by the 2^{nd} order linear interpolation (Gaussian), divergence terms were solved by the 2^{nd} order upwind interpolation (Gaussian) and Laplacian terms were solved by the 2^{nd} order linear interpolation with explicit non-orthogonal corrections. To improve the stability of the computations, the relaxation parameters (which limit the variable changes from one iteration to the next iteration) are set to 0.3 for pressure and 0.5 for the other variables.

The PIMPLE method was used for the pressure-velocity coupling. PIMPLE algorithm combines the PISO (pressure implicit with splitting of operators) and SIMPLE (semi-implicit method for pressure-linked equations) algorithms to rectify the second pressure correction and correct both velocity and pressure explicitly. This algorithm allows one to use larger time steps than the PISO algorithm. Due to the transient conditions of flow in the ABL, an adaptive time-stepping technique based on Courant-Friedricks-Lewy-number (CFL-number) is used (Bechmann, 2006):

$$CFL = \Delta t_{max}\left(\frac{|u|}{\Delta x}, \frac{|v|}{\Delta y}, \frac{|w|}{\Delta z}\right) \leq 1 \tag{26}$$

where u, v and w are the velocity components in $x-$, $y-$ and $z-$directions respectively. In this study after studying the results of the model for different sets of CFL, the maximum value of global CFL is adopted to 0.5. For larger time steps, numerical dissipation increases as the CFL-number increases and the model becomes more unstable (Wang, 2013; Ferziger and Perić, 2002).

The problems that arise in solving these equations are memory related issues and also the run time (to obtain a solution) when running the model. As stated earlier on, the core of the model is based on OpenFOAM, and therefore the framework offers parallelization features. Hence, the model can be decomposed and ran on a relatively large number of processors, either on supercomputers or HPC clouds to reduce the simulation time.

Usually due to the limitation of computational resources, it is not possible to use a very fine mesh or very small time steps in simulations. In this study different settings for numerical schemes and mesh sizes as well as time steps were considered to determine the optimal balance between the needed computational resources and the desired accuracy. In the real case simulations presented in Section (6), the time step values varied between 0.1 and 10.0 s(i.e. $0.1 \leq \Delta t \leq 10.0\ s$) and 30 h of simulations, as described in Section (6), took about 12 h on the HPC Cloud-based virtual machine with 24 Intel processors at 2.7 GHz and 96 GB RAM (Collaborative Organisation for ICT in Dutch Higher Education and Research, 2017).

3. Computational domain

Computational domain is extended 3,500 m in $x-$ direction, 1,850 m in $y-$ direction and more than 500 m upwards ($z-$direction) in order to allow the flow to settle and avoid interaction between boundary conditions and the developing flow (Joubert et al., 2012; Prospathopoulos and Voutsinas, 2006; Vinnichenko et al., 2011). As shown in Fig. 2, the extension of the computational domain downwind of the water body is larger than the upwind distance to minimize the effects of outflow boundary on the airflow. The shape of the water surface is the primary input for building the computational domain in the current simulation. The water surface shape, though relatively small, induces complex 3D flow in ABL. During the simulation time (one day), changes of the water level with an average value of 0.006 m were ignored and a constant level was assumed for the water surface. The water surface shape was generated from the roughly measured bathymetry using the approach proposed by Abbasi et al. (2017a).

3.1. Mesh generation

Generating and applying a good computational grid is a very important step in performing reliable CFD simulations especially in complex terrains. Generally, in ABL simulations, grid generation remains a significant challenge for CFD simulations. Using a computational grid with highly skewed, non-orthogonal differential cells will produce significant errors in solving the governing equations. Indeed, meshing complex terrains is not straightforward and is very case-sensitive especially for heterogeneous surfaces with sharp changes in their properties. The generated mesh must accurately represent the shape of the water surface and its

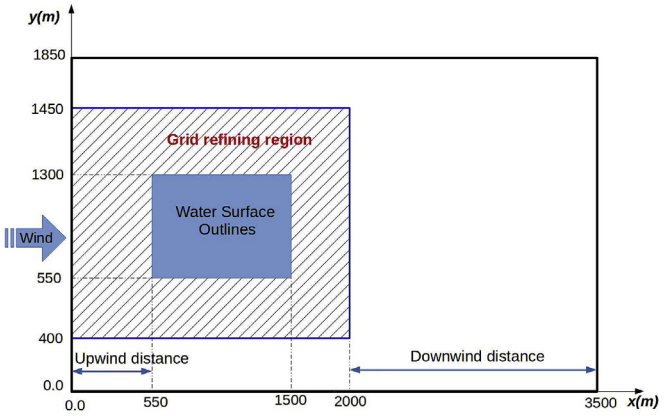

Fig. 2. Plan view of computational domain, water surface outlines and grid refining region.

surrounding terrain. To improve the generated computational grid, concentration of grid points near the lake's boundary and near the bottom boundary (wall) are more clustered to cover the sharp changes in surface properties. Refining the computational mesh only at specific regions can reduce significantly the computational cost (Prospathopoulos et al., 2012). In addition, refining the grid at regions with abrupt changes in surface characteristics increases the representation accuracy of the terrain and the predictions accuracy as well. The quality of the mesh has a clear impact on the accuracy of any CFD simulation (Rhoads, 2014) and affects significantly the convergence speed and the accuracy of the modeling.

The proposed framework uses a right hand coordinate system (typically used in simulations), with the $z-$axis positive in the upward direction (normal to the water surface). The origin is located in the lower left-hand corner of the mesh when viewed in the $xy-$plane. Keeping with this convention in the model, the $x-$axis is aligned to be positive in the easterly direction, with the $y-$axis positive in the northerly direction. Horizontal grids are generated by following the geometrical boundaries (water surface and land) available in the computational domain. For the vertical direction the grid points are clustered near the water surface and at the location of abrupt changes to resolve the turbulent flow field and capture flow parameters such as temperature and shear stress distributions in the most dynamic zones. Fig. 3 shows the generated grid details. The vertical grids near the lower surface should be sufficiently fine to be able to capture the large thermal and velocity gradients present in this region.

In this work, the computational grid was generated with snappyHexMesh (sHM) utility available in OpenFOAM. sHM is a powerful script-driven tool, which generates unstructured mesh containing hexahedra and split-hexahedra cells (Brockhaus, 2011). snappyHexMesh proved to be very flexible with different domain configurations. sHM allows to use STL (STereoLithography/Standard Triangle Language) files which represent the small water surfaces in complex heterogeneous surfaces. Although using unstructured meshes allows for local mesh refinement and facilitates the transition between regions with different mesh densities, they are more costly than structured meshes. Unstructured meshes are being used widely in ABL simulations due to their flexibility and the adaptation capability (Kim and Boysan, 1999). The final mesh used in this simulation consists primarily of hexahedral cells (1, 144, 900 cells) with some polyhedral cells (17, 268 cells). The choice of mesh size is based on the available computational resources and the resolution required to get accurate results as well. This mesh has to be refined sufficiently near the bottom boundary (Abbasi et al., 2017a). The final computational grid is shown in Fig. 4.

In the current simulation, the effect of the roughness of surfaces is applied by using wall functions which introduce some restrictions on the minimum height of the first cell above the bottom surface. This requires the first cell center adjacent to the wall not to be smaller than the roughness height (it means it should be placed within the logarithmic region of the boundary layer) (Joubert et al., 2012; Wakes et al., 2010). According to the roughness lengths of the bottom surfaces (land and water surface) the height of the first cells near the wall could be very large (a cell size of 3.5 and 0.25 m should be chosen for the cells adjacent to the land and water surface respectively), and with this cell size, there would be big errors in simulations. To overcome this problem, the first cell placed on top of the roughness elements and the boundary conditions should be modified. Displacing the first model level by z_0 (where z_0 is the surface roughness length) has the advantage that in the case of large roughness changes (e.g. land) there are no minimum height restrictions for the first cells (Koblitz et al., 2015).

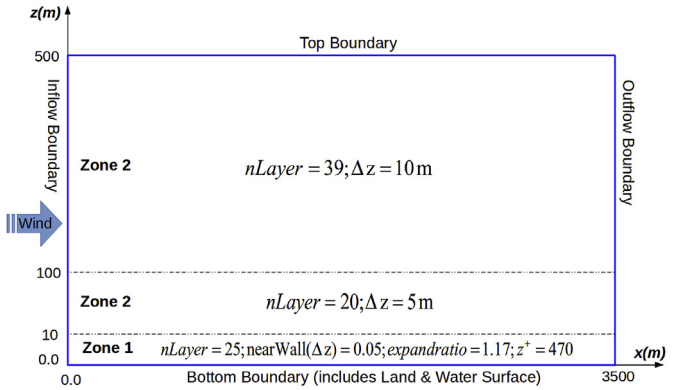

Fig. 3. Defined different zones in height ($z-$direction) to generate computational grid. Properties of generated mesh in each zone are presented.

4. Initial and boundary conditions

4.1. Initial conditions

Even if the initial conditions may have little effects on the final results of the simulations, it is strictly suggested to assign real initial conditions in the model. Implementing correct initial conditions in the model could be useful in converging the simulations and reduce the simulation time specially for first time steps. As in most cases, often there is no sufficient data to generate the initial distribution of airflow parameters, therefore the vertical profiles in the inflow at the start time of simulation (at $t = 0$) are used throughout the entire domain as initial condition (Section (5)). Setting the initial condition (simple or complex) is done using the funkySetField tool available in swak4Foam libraries, which are python-based functions applicable alongside OpenFOAM. To prevent the numerical instabilities, for turbulence parameters, it is suggested to impose a weak initial turbulence level (a non-zero turbulence condition) in ABL simulations (Verdier-Bonnet et al., 1999).

4.2. Boundary conditions

As shown in Fig. 4, the modeled computational domain has seven defined physical boundaries: Inflow boundary as the upwind boundary; Outflow as the downwind boundary; two boundaries parallel to the wind direction (Back and Front); two walls to represent the water surface (Water Surface) and the surrounding terrain (Terrain); and the Top boundary as the vertical extension of the domain.

4.2.1. Inflow boundary

As measurements available in most ABL studies are not

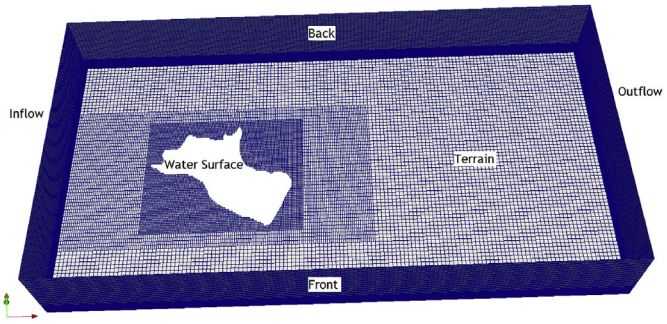

Fig. 4. Computational grid and boundaries of the model. Top boundary and water surface are not shown to make a better view.

sufficient to determine the velocity field at the inflow boundary of the computational domain, the logarithmic law is used for the vertical distribution of the inflow velocity, assuming neutral atmospheric conditions. The vertical profiles should represent the characteristics of upstream terrain (Blocken et al., 2007; Prospathopoulos and Voutsinas, 2006). The use of the logarithmic velocity profile in this region where the inflow and bottom boundary meet would improve the stability of the simulation. Inflow boundary conditions for u_i, k and ε respectively are given by the following equations (Blocken et al., 2007; Joubert et al., 2012; Yang et al., 2009):

$$u = \frac{u_*}{\kappa}\ln\left(\frac{z+z_0}{z_0}\right); \qquad v = 0; \qquad w = 0; \tag{27}$$

$$k = \frac{u_*^2}{\sqrt{C_\mu}}\sqrt{C'_1 \times \ln\left(\frac{z+z_0}{z_0}\right) + C'_2} \tag{28}$$

$$\varepsilon = \frac{u_*^3}{\kappa(z+z_0)}\sqrt{C'_1 \times \ln\left(\frac{z+z_0}{z_0}\right) + C'_2} \tag{29}$$

where u_* is the friction velocity $[ms^{-1}]$ given by:

$$u_* = \frac{u_{ref}\kappa}{ln\left(\frac{z_{ref}+z_0}{z_0}\right)}; \tag{30}$$

where u, v and w are velocity components in $x-$, $y-$ and $z-$directions respectively, κ is the von Karman constant (≈ 0.4187), z_0 is the aerodynamic roughness length $[m]$, z is the vertical distance above the bottom surfaces $[m]$, C'_1, C'_2 and C_μ are constant where $C'_1 = -0.01$, $C'_2 = 1.23$ and $C_\mu = 0.033$ (OSullivan et al., 2011), and u_{ref} is the wind speed measured at the reference height (z_{ref}). In the vertical profiles of the mean horizontal wind speed U, turbulent kinetic energy k and turbulent dissipation rate ε described, it is assumed that the ABL is in neutral condition (i.e. the turbulence originates from friction and shear forces and the effect of thermal stratification are ignored) (Yang et al., 2009). If the measurements of the atmospheric stability conditions are available, the profiles can be modified to take into account the real conditions at inflow boundary (Section (5)). In this study, the roughness length for the terrain surrounding the water surface (lake) is assumed $z_0 = 0.13\,m$, which represents a land surface with sparse vegetation (Bagayoko et al., 2007).

For temperature, according to the approach used for setting the stability conditions in the simulation (Section (2.3)), either the modified vertical temperature profile (considering the stability effects as shown in Equation (36)) or simple vertical profile (considering only the lapse rate) can be used. As the temperature values were available for land and water surfaces, therefore, the vertical temperature profile including the lapse rate term was used as inlet boundary condition.

4.2.2. Top boundary

The top boundary is positioned high enough (about $500\,m$) above the top of the boundary layer and the no-flux condition can be imposed for the velocity field (Churchfield, 2013; Prospathopoulos and Voutsinas, 2006). Physically in this boundary condition, the velocity is tangential to the boundary as follows:

$$u = U_\infty; \quad v = w = 0; \quad \frac{\partial k}{\partial z} = 0; \quad \frac{\partial \varepsilon}{\partial z} = 0; \quad \frac{\partial q}{\partial z} = 0; \quad T = T_\infty \tag{31}$$

where u, v and w are velocity components in $x-$, $y-$ and $z-$directions respectively, U_∞ and T_∞ prescribing the values corresponding to the inflow velocity and inflow temperature profiles respectively, at the height of the top boundary. For other flow variables, it is assumed that the fluxes across the top of the domain are zero and hence symmetry conditions (no-gradient) are used.

4.2.3. Outflow boundary

At outlet boundary, the flow that leaves the domain is typically not known before solving the flow. However, in most ABL simulations fully developed flow conditions (zero-normal gradient conditions) are imposed on the outflow boundary which introduce errors (Benjamin et al., 2011; Hussein and El-Shishiny, 2009). As the flow in homogeneous ABL is not fully developed, this assumption introduces some errors in the flow parameters. To minimize the errors due to this assumption, the outflow boundary is placed far downstream of the area of interest (water surface) (Koblitz et al., 2015). The following conditions are assumed as boundary conditions at the outflow:

$$\frac{\partial u}{\partial x} = 0; \quad \frac{\partial v}{\partial x} = 0; \quad \frac{\partial w}{\partial x} = 0; \quad \frac{\partial k}{\partial x} = 0; \quad \frac{\partial \varepsilon}{\partial x} = 0; \quad \frac{\partial q}{\partial x} = 0; \quad \frac{\partial T}{\partial x} = 0 \tag{32}$$

4.2.4. Lateral boundaries

For the lateral boundaries (Back and Front) which are oriented parallel to the wind direction, slip boundary condition is imposed which represents the fully developed flow conditions on the lateral boundaries (Prospathopoulos and Voutsinas, 2006):

$$\frac{\partial u}{\partial y} = 0; \quad v = 0; \quad \frac{\partial w}{\partial y} = 0; \quad \frac{\partial k}{\partial y} = 0; \quad \frac{\partial \varepsilon}{\partial y} = 0; \quad \frac{\partial q}{\partial y} = 0; \quad \frac{\partial T}{\partial y} = 0 \tag{33}$$

As shown in Equation (33), slip boundary represents a zero-gradient condition for scalar parameters (such as k and ε) and for the tangential components of velocity vector (i.e. u and w) and defines fixed value (zero) for the normal component (i.e. v) of velocity.

4.2.5. Bottom boundary

In the desired computational domain, the bottom boundary encompasses two surfaces with different properties, land surface and water surface. Heterogeneous surfaces which contain different surfaces, make the airflow over the surface complex. Wind flow over the heterogeneous surfaces is strongly affected by the surfaces roughness length. In order to simulate airflow over the water surface and its surrounding accurately, the boundary conditions for bottom surfaces must be correctly selected (Luna et al., 2003; Wakes et al., 2010). The lower boundary conditions (water and land surfaces) use wall functions. Using the wall functions, the airflow is not solved explicitly in the immediate vicinity of the bottom surface and the effects of surfaces on the airflow are modeled through wall function by using proper aerodynamic roughness length (z_0) values (Foudhil et al., 2005).

Using a wall function besides RANS simulation of the ABL has the limitation of inconsistency between the standard wall function formulation and the fully developed inflow conditions for ABL (Balogh et al., 2012). Generally, to resolve this limitation, it is required that the vertical distance of the first cell's center point (z_p) of the wall-adjacent cell (bottom boundary) should be larger than the physical roughness height (k_s) of the surface ($z_p \gtrsim k_s$) (Blocken et al., 2007). Physically, it is not meaningful to have grid cells within the physical roughness height (Benjamin et al., 2011;

Table 1
Parameters describing different stability conditions in validating cases (adopted from Pieterse (2013)).

ABL state	$z_0[m]$	$u_r[ms^{-1}]$	$z_r[m]$	$q_0[Wm^{-2}]$	$T_0[C]$	$L[m]$	$u_*[ms^{-1}]$	κ	$k_s[m]$
Neutral	0.002	10	10	0.0	25.0	∞	0.481	0.41	0.015
Stable	0.002	10	10	−30.0	10.0	309.5	0.472	0.41	0.015
Unstable	0.002	10	10	100.0	40.0	−108.1	0.497	0.41	0.015

Blocken et al., 2007).

The physical roughness height (k_s) is a function of the aerodynamic (momentum) roughness length (z_0) of the surface and can be computed as follows (Prospathopoulos and Voutsinas, 2006):

$$k_s = \frac{E}{C_s} z_0 \tag{34}$$

where E represents the empirical constant (≈ 9.793) and C_s is the roughness constant which contains the type of roughness. Due to the lack of specific guidelines on determining the value of roughness constant, generally its default value for sand-grain roughened pipes and channels (≈ 0.5) is used (Blocken et al., 2007).

Using standard wall functions in one hand, requires a refinement of the mesh near the rough wall to capture the high gradients in flow parameters, and on the other hand, introduces the constraint of placing the first computational node at least k_s away from the wall. To resolve this contradictions, the roughness height (z_0) is included in the vertical profiles of the inflow boundary conditions presented in Equation (27) through Equation (30). By setting these inflow boundary conditions, the first cell can be displaced on top of the roughness elements (z_0) and therefore, in the case of large roughness changes (e.g. water to land) there are no minimum height restrictions for the first cell (Koblitz et al., 2015).

Changes in surface roughness (from dry land to water surface) cause the local profiles of wind speed, temperature and turbulence to be out of equilibrium and make the flow fully three-dimensional and more complex than flow over a flat terrain. For the surrounding lands, due to the low to moderate wind speed values, the changes of roughness with wind speed are ignored. Therefore, the average roughness length assumed is $z_0 = 0.13\ m$, which represents a land surface with sparse vegetation (Prospathopoulos et al., 2012; Bagayoko et al., 2007). For the water surface, the roughness length was assumed $z_0 = 10^{-4}\ m$ which seems to be appropriate on this type of water surfaces with low to moderate wind speed (Vercauteren, 2011).

For temperature boundary condition over the bottom surface, the measured surfaces temperature (for both water and land surface) can be used directly (Dirichlet boundary condition), or the heat flux values can be specified (Neumann boundary condition). Changes in temperature of bottom surface might occur mainly due to the heat exchange across the bottom surface and air interface. Accurate estimation of heat fluxes is extremely important in the simulation of temperature dynamics over the ground (bottom) surface (Abbasi et al., 2017b). In this study, however, both approaches for temperature boundary conditions stated above can be used, but the measured surfaces temperature values were used in the simulation of lake Binaba. Obviously, using the Dirichlet boundary condition for temperature on the bottom surface has less uncertainties and could decrease the computational time. For the above mentioned approaches and their details, especially over the water surface, the reader is referred to Abbasi et al. (2017a, 2016).

5. Validation of the model

The main aim of using numerical models in ABL simulations is to provide predictions that represent the real air flow field with a reasonable accuracy (Wakes et al., 2010). Generally, to validate a numerical simulation, accurate measured data from full-scale

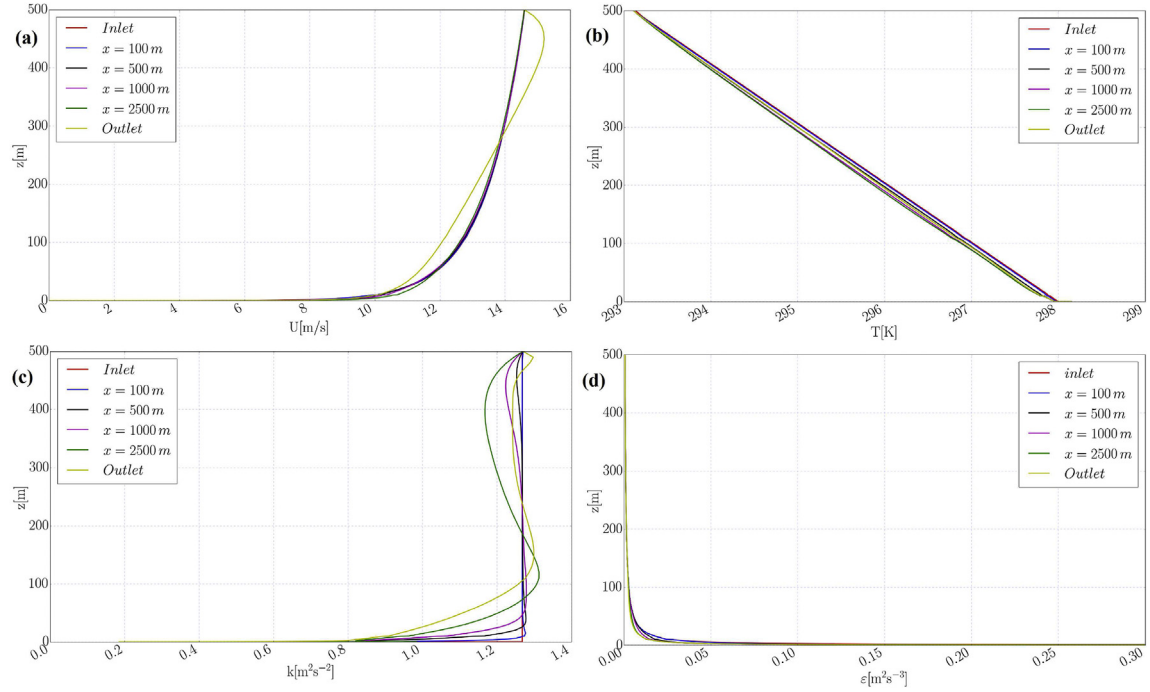

Fig. 5. Neutral model results illustrating streamwise gradients for **(a)** wind speed; **(b)** temperature; **(c)** turbulent kinetic energy; and **(d)** turbulent dissipation rate.

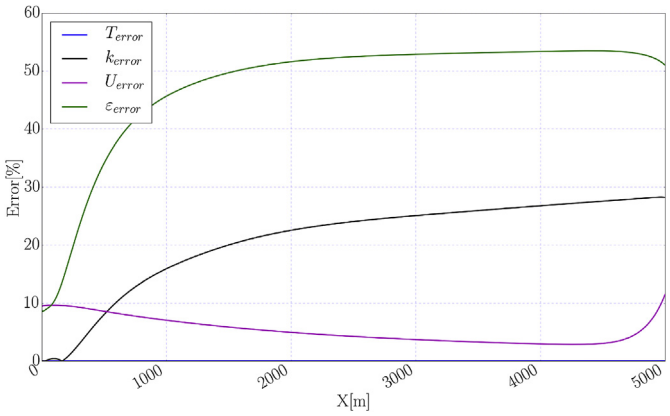

Fig. 6. Relative change of flow parameters in neutral condition relative to the inlet values.

observations are necessary. In ABL modeling, because of the practical difficulties in taking full-scale measurements, these measurements are rare (Kim and Patel, 2000). In the current study, to validate the solver developed, the turbulence models for different atmospheric stability conditions and the performance of the boundary and initial conditions set, three models with different stability conditions according to Pieterse (2013) were selected. The details of the validated cases are summarized in Table 1. To validate the model using the pre-described parameters in Table 1, the computational mesh, initial conditions, and turbulence model equations were adopted from Pieterse (2013). As in these cases the stability parameters are known, the first approach (free stream stability approach) described in Section (2.3) was used to set stability conditions in the simulations. Hence, the inlet profiles were modified as below:

$$u(z) = \frac{u_*}{\kappa}\left[\ln\left(\frac{z+z_0}{z_0}\right) - \Phi_m(\zeta)\right] \tag{35}$$

$$T(z) = \frac{T_*}{\kappa}\left[\ln\left(\frac{z+z_0}{z_0}\right) - \Phi_h(\zeta)\right] + T_0 - z\frac{g}{C_p} \tag{36}$$

where $\zeta = \frac{z}{L}$ is the stability parameter, L is the Monin-Obukhov length and is defined as:

$$L = \frac{u_*^2 T_0}{\kappa g T_*} \tag{37}$$

where C_p is the specific heat of air, g is the gravity acceleration, T_0 is the temperature at ground level and T_* is the scaling temperature defined as

$$T_* = \frac{-q_0}{\rho C_p u_*} \tag{38}$$

where q_0 is the heat flux from the surface, ρ is air density, Φ_h and Φ_m are the integrated forms of the similarity functions and are given by

$$\Phi_h = \Phi_m = -5\frac{z}{L} \qquad L > 0; \tag{39}$$

$$\Phi_m = \ln\left[\left(\frac{1+x^2}{2}\right)\left(\frac{1+x}{2}\right)^2\right] - 2\tan^{-1}x + \pi/2 \qquad L < 0 \tag{40}$$

$$\Phi_h = 2\ln\left(\frac{1+x^2}{2}\right) \qquad L < 0; \tag{41}$$

where

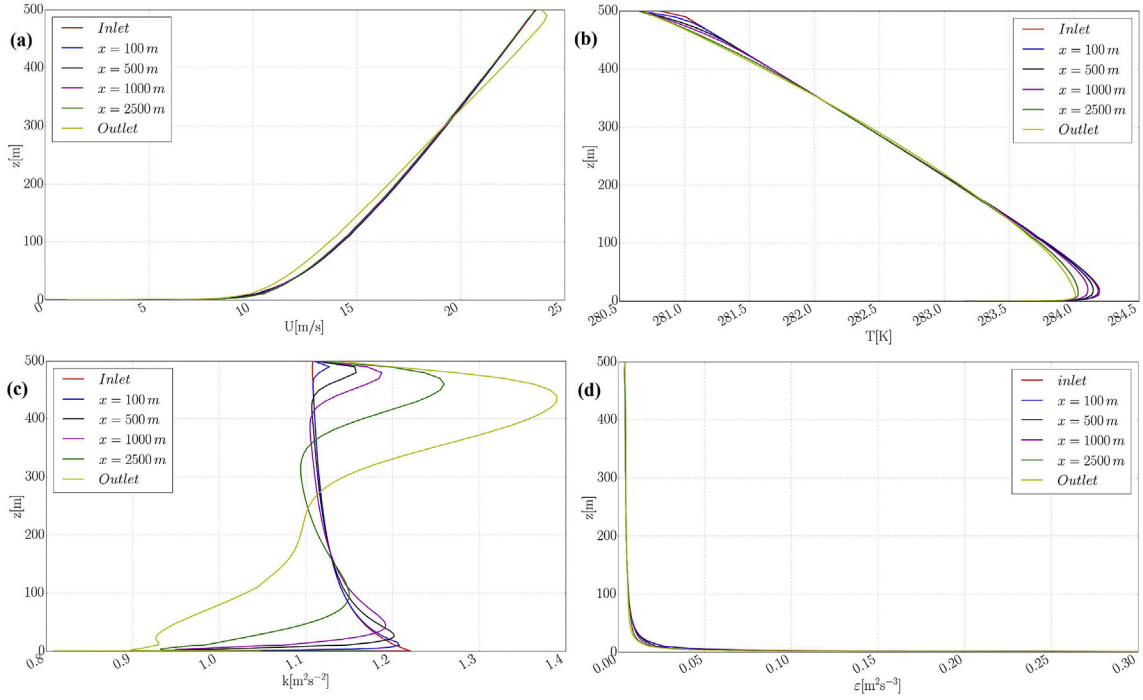

Fig. 7. Model results for stable atmospheric condition illustrating streamwise gradients for **(a)** wind speed; **(b)** temperature; **(c)** turbulent kinetic energy; and **(d)** turbulent dissipation rate.

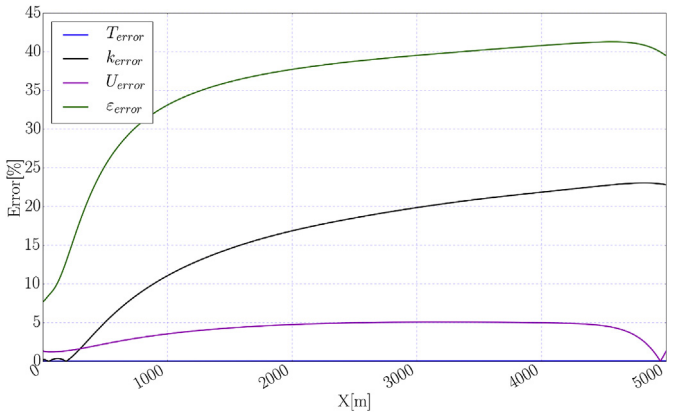

Fig. 8. Relative change of flow parameters in stable atmospheric condition relative to inlet values.

Fig. 10. Relative change of flow parameters in unstable atmospheric condition relative to inlet values.

$$x = \left(1 - 16\frac{z}{L}\right)^{1/4} \tag{42}$$

For turbulence parameters, the inlet profile considering the stability conditions could be written as

$$\varepsilon(z) = \frac{u_*^3}{\kappa z}\varphi_\varepsilon\left(\frac{z}{L}\right) \tag{43}$$

$$k(z) = \sqrt{\frac{\nu_t \varepsilon}{\rho C_\mu}} - 5.48u_*^2\sqrt{\frac{\varphi_\varepsilon(z/L)}{\varphi_m(z/L)}} \tag{44}$$

where ν_t is turbulent kinematic viscosity and φ_ε is given by:

Fig. 11. Lake Binaba and its surroundings.

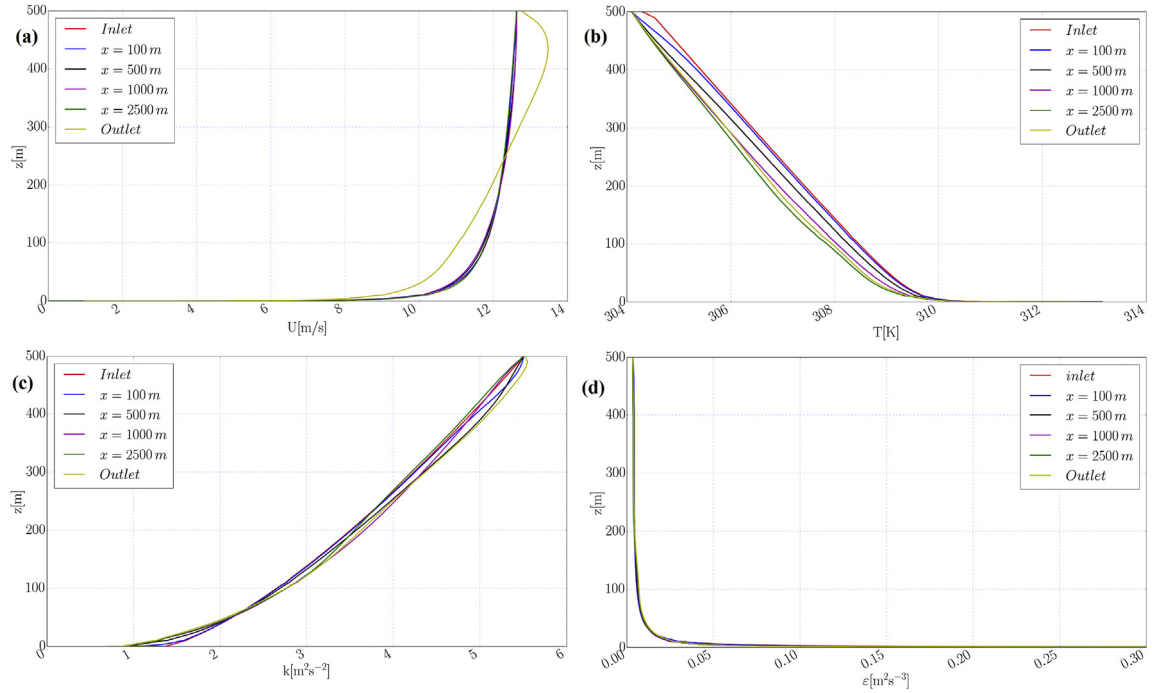

Fig. 9. Model results for unstable atmospheric condition illustrating streamwise gradients for **(a)** wind speed; **(b)** temperature; **(c)** turbulent kinetic energy; and **(d)** turbulent dissipation rate.

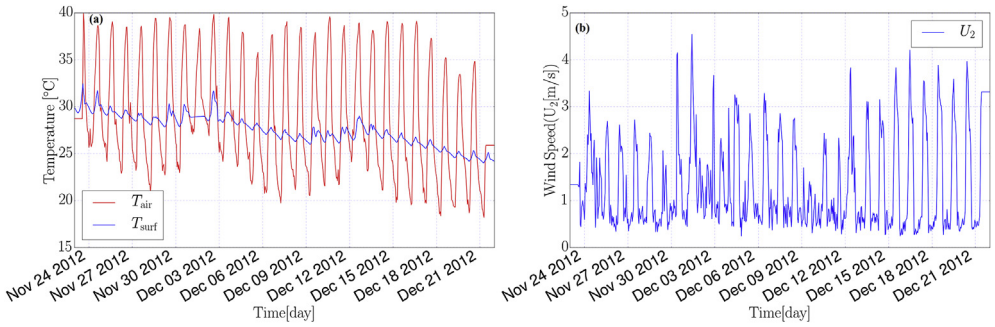

Fig. 12. **(a)** Measured water surface and air temperature at 2 *m* above water surface; **(b)** measured wind speed at 2 *m* above water surface during the simulation period.

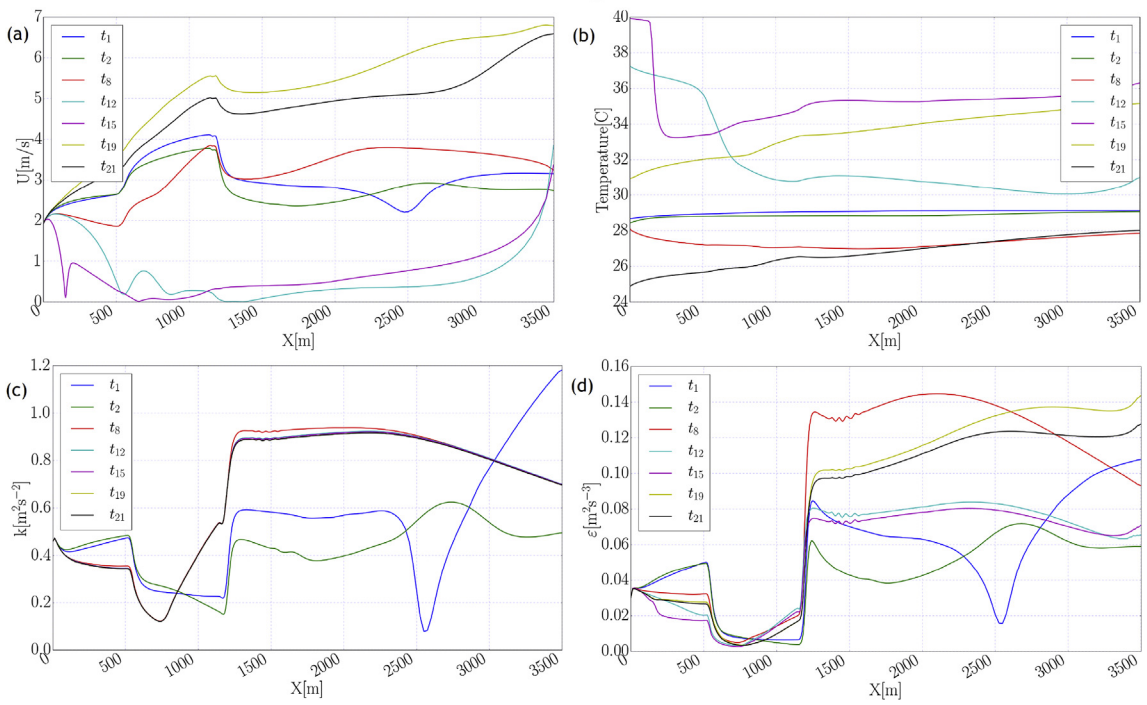

Fig. 13. Simulated flow parameters at height 2 *m* above the bottom surface in streamwise ($x-$)direction includes land and water surface. Water surface extends from $x \approx 550$ to $x \approx 1200$ *m*. Results are plotted for seven different times: $t_1 = 01:00$, $t_2 = 02:00$, $t_8 = 08:00$, $t_{12} = 12:00$, $t_{15} = 15:00$, $t_{19} = 19:00$ and $t_{21} = 24:00$ *hr*: **(a)** velocity; **(b)** temperature; **(c)** turbulent kinematic energy; and **(d)** dissipation rate of turbulent kinetic energy.

$$\varphi_\varepsilon\left(\frac{z}{L}\right) = \begin{cases} 1 - \dfrac{z}{L} & \text{if} \quad L < 0, \\ \varphi_m\left(\dfrac{z}{L}\right) - \dfrac{z}{L} & \text{if} \quad L > 0 \end{cases} \tag{45}$$

φ_h and φ_m are the similarity functions and are given by:

$$\begin{cases} \varphi_m = \varphi_h = 1 + 5\dfrac{z}{L} & \text{if} \quad L > 0, \\ \varphi_m^2 = \varphi_h = \left(1 - 16\dfrac{z}{L}\right)^{-1/2} & \text{if} \quad L < 0 \end{cases} \tag{46}$$

As the bottom boundary is homogeneous, the prescribed cases for the validation were run in 2D. It is assumed that there is an

Table 2
Selected time windows of the model to present the results which include both stable and unstable atmosphere (ζ is stability parameter calculated over the water surface, T_a is air temperature, T_{ws} is water surface temperature, and T_{ref} is reference temperature).

Time[*hr*]	$\zeta[-]$	$T_a[K]$	$T_{ws}[K]$	$T_a - T_{ws}[K]$	$T_{ref}[K]$	$T_a - T_{ref}[K]$	Stability Condition
11	−1.13	301.81	302.02	−0.21	293.15	8.81	Unstable
2	−3.48	301.58	301.94	−0.36	293.15	8.58	Unstable
8	−2.95	301.21	301.82	−0.61	293.15	8.21	Unstable
12	2.11	310.4	303.72	6.68	293.15	17.4	Stable
15	4.75	313.08	305.15	7.93	293.15	20.08	Stable
19	−3.17	304.13	303.64	0.49	293.15	11.13	Unstable
24	−9.5	297.99	301.74	−3.75	293.15	4.99	Unstable

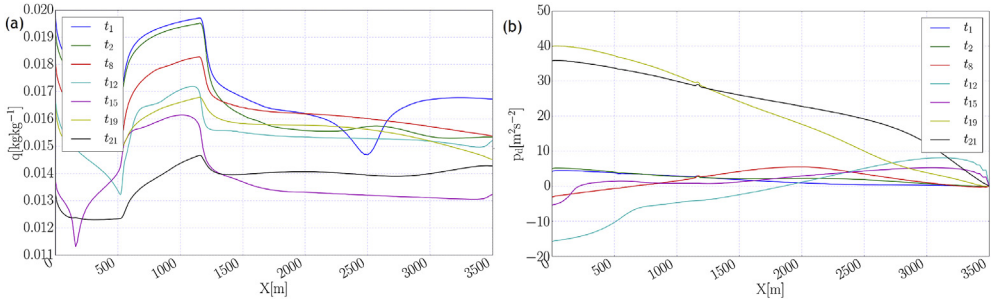

Fig. 14. Simulated flow parameters at height 2 *m* above the bottom surface in streamwise ($x-$)direction include land and water surface. Water surface extends from $x \approx 550$ to $x \approx 1200$ m. Results are plotted for seven different times: $t_1 = 01:00$, $t_2 = 02:00$, $t_8 = 08:00$, $t_{12} = 12:00$, $t_{15} = 15:00$, $t_{19} = 19:00$ and $t_{21} = 24:00$ *hr*: **(a)** specific humidity; and **(b)** dynamic pressure ($P_d = P_{total} - P_{static}$).

equilibrium ABL which implies horizontal homogeneity, this implies the streamwise gradients of all parameters should be zero (Yang et al., 2009). It also means that by comparing the imposed profiles at the inflow boundary and the predicted profiles in different positions streamwise, it is possible to validate the model. Theoretically, the vertical profiles should be maintained throughout a computational domain without an obstacle.

Using the assumption of equilibrium ABL, the vertical profiles of airflow parameters in each prescribed validation case are plotted. The streamwise flow parameters under neutral condition are illustrated in Fig. 5. It can be seen that the vertical

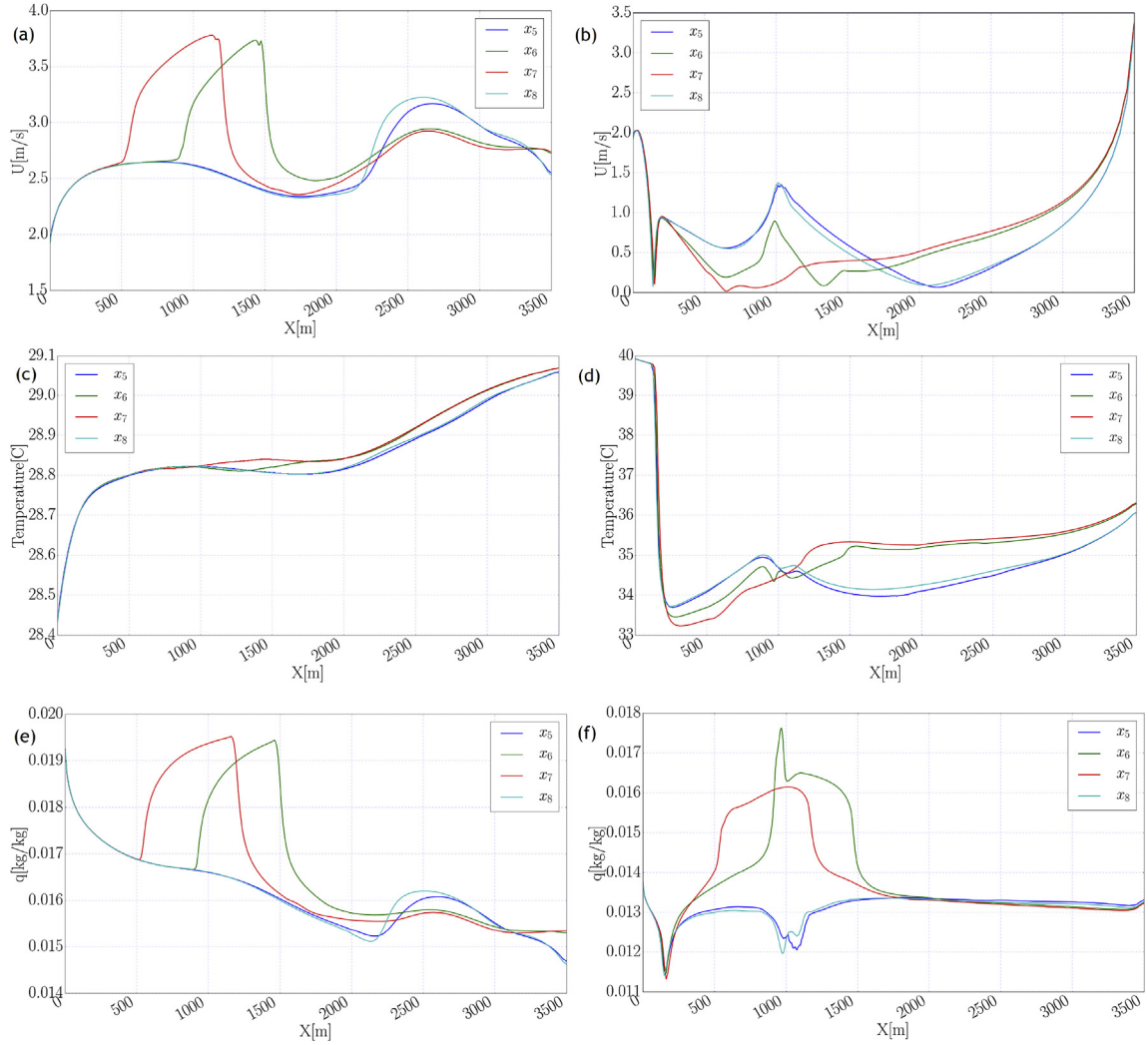

Fig. 15. Comparison of simulated flow parameters at height 2 *m* above bottom surface in streamwise ($x-$)direction for different conditions: x_5: includes only land surface, x_6: includes land and water surface extending from $x \approx 900$ to $x \approx 1300$ *m*, x_7: includes land and water surface extending from $x \approx 550$ to $x \approx 1200$ *m*, x_8: includes only land surface: **(a)** velocity at $t = 02:00$ *hr*; **(b)** velocity at $t = 15:00$ *hr*; **(c)** temperature at t = 02:00 hr; **(d)** temperature at $t = 15:00$ *hr*; **(e)** specific humidity at $t = 02:00$ *hr*; **(f)** specific humidity at $t = 15:00$ *hr*.

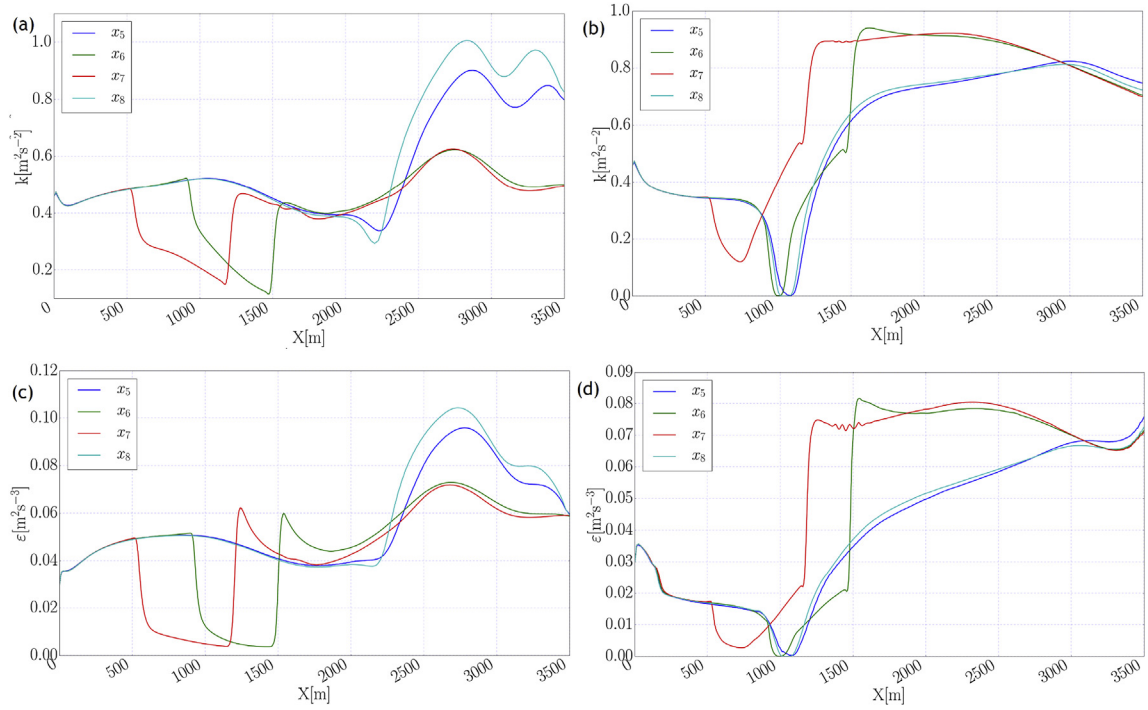

Fig. 16. Comparison of simulated flow parameters at height 2 m above bottom surface in streamwise ($x-$)direction for different conditions: x_5: includes only land surface, x_6: includes land and water surface extending from $x \approx 900$ to $x \approx 1300$ m, x_7: includes land and water surface extending from $x \approx 550$ to $x \approx 1200$ m, x_8: includes only land surface: **(a)** turbulent kinetic energy at $t = 02:00$ hr; **(b)** turbulent kinetic energy at $t = 15:00$ hr; **(c)** dissipation rate of turbulent kinetic energy at $t = 02:00$ hr; **(d)** dissipation rate of turbulent kinetic energy at $t = 15:00$ hr.

profiles of the flow are maintained throughout the downstream distance. There are some slight differences which are consistent with the observation of previous studies (e.g. Blocken et al. (2007); Hargreaves and Wright (2007); Pieterse (2013)). A comparison of the homogeneity error at a height of 10 m, relative to the inlet conditions under neutral atmosphere is shown in Fig. 6. It illustrates clearly that the temperature profile is well maintained. The maintenance of the velocity is also particularly good, with less than 10% error at a height of 10 m, the point in the domain where some of the largest inhomogeneities were observed (Pieterse, 2013). The relative streamwise large gradients in the k and ε profiles could be mainly due to the use of wall functions and has been investigated by many researchers (e.g. Blocken et al. (2007); Hargreaves and Wright (2007); Parente et al. (2011)). The streamwise gradients of flow parameters under stable and unstable atmosphere are shown in Fig. 7 and Fig. 9 respectively. Similar to the neutral simulation, the comparison of the homogeneity error at a height of 10 m, relative to the inlet conditions under stable and unstable atmosphere is shown in Fig. 8 and Fig. 10 respectively. As shown in these graphs, the model performance is better in the non-neutral atmosphere. Generally, the performance of the model regarding the stability conditions is good and could be used in simulating the airflow in ABL considering stability conditions. For more details about the validating process and the results refer to Pieterse (2013).

6. Description of study site and data collection

The Upper East Region of Ghana is classified as one of the poorest in the country. Most of the inhabitants of the region (mostly rural areas) are farmers and rely on rainfed agriculture. To improve their livelihoods and enhance food security a number of small reservoirs (more than 160) with surface areas between 1 and 100 hectares (Abbasi et al., 2016; Annor et al., 2009) were constructed for them by the Ghana government and development partners in the late 1980s and early 1990s. These were constructed to promote dry season farming (crop and livestock), fishing and domestic water uses. Their closeness to the point of use made them very attractive (Abbasi et al., 2017c; Keller et al., 2000). However with recent changes in climate (climate change), the small reservoirs which were to increase the resilience of the communities which use them are at risk from high evaporation losses from them. Binaba dam, a small and shallow reservoir located in this region ($10^\circ 53'20''N$, $00^\circ 26'20''W$) was studied to determine the rate of heat fluxes in small lakes in this region. The Binaba reservoir has an average surface area of 31 ha with a maximum and average depth of 4.0 m and 1.1 m respectively, at full storage level (Fig. 11). To monitor the meteorological parameters, a floating measurement station was installed over the water surface. Measurements taken included atmospheric parameters (air temperature, wind speed at 2 m above the water surface, wind direction and relative humidity), incoming shortwave radiation, water temperature profile, and sensible heat flux using a 3-D sonic anemometer. The installed 3-D sonic anemometer recorded sensible heat flux over the water surface at 10 Hz and accumulated over 30-minutes intervals. The air temperature fluctuated from 18.0 to 40.0° C with an average of 28.7° C while the water surface temperature varied between 24.0° C and 32.5° C with an average of 27.5° C during the measurement period. Measurements were done from November 23, 2012, to December 22, 2012. Fig. 12(a) shows the diurnal changes of air temperature, with daily variations of approximately 10.0° C. The maximum wind speed recorded during the study was 4.5 ms^{-1} (Fig. 12(b)) with the South-Western direction being the most dominant direction.

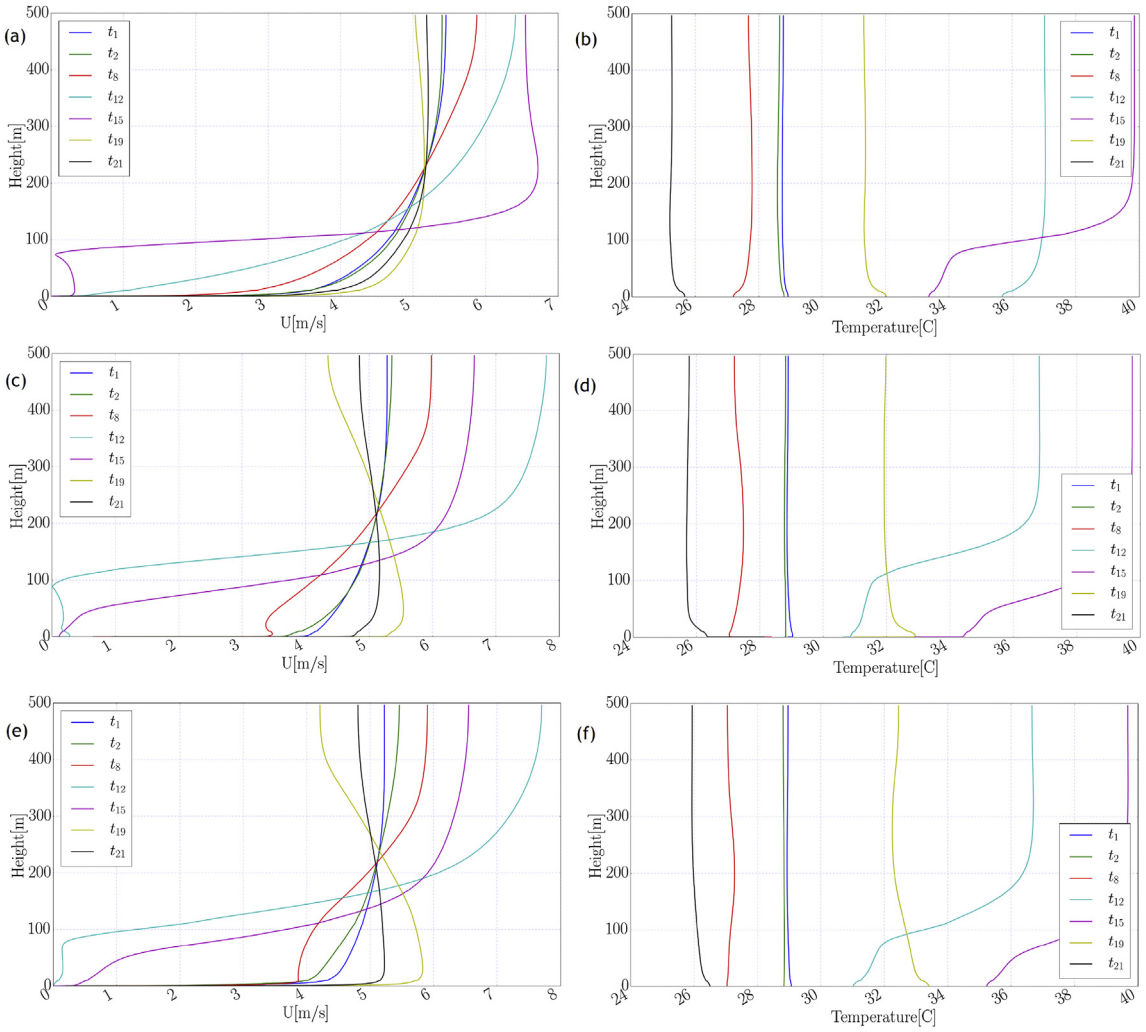

Fig. 17. Comparison of the simulated flow parameters in height ($z-$direction) for different locations in streamwise direction and for different times:$t_1 = 01:00$, $t_2 = 02:00$, $t_8 = 08:00$, $t_{12} = 12:00$, $t_{15} = 15:00$, $t_{19} = 19:00$ and $t_{21} = 24:00$ hr: **(a)** velocity at x = 500 m on land in upstream of the water surface; **(b)** temperature at x = 500 m on land in upstream of the water surface; **(c)** velocity at x = 1000 m over the water surface; **(d)** temperature at x = 1000 m over the water surface; **(e)** velocity at x = 1300 m on land in downstream of the water surface; **(f)** temperature at x = 1300 m on land in downstream of the water surface.

7. Results and discussion

To simulate the transient behavior of ABL and the influence of water surface on the airflow, unsteady RANS (URANS) was used (Equation (1) through (Equation (4)). In the following section, by using the results of the model, the effects of water surface on the flow features in ABL is discussed. To this end, the flow parameters such as velocity, temperature and water vapor concentration over the water surface and its surroundings are analysed.

In the modeled complex domain, the airflow encounters sudden changes in surface roughness, temperature and wetness. These sharp changes modify the velocity, humidity and temperature profiles in a layer near the bottom boundary which is commonly referred to as the Internal Boundary Layer (IBL) (Bou-Zeid et al., 2004; Józsa et al., 2007).

In Fig. 13 the flow parameters in streamwise ($x-$)direction that includes both land (upstream and downstream) and water surface, are plotted at different times. As shown in the velocity graph (Fig. 13(a)) the flow velocity has sharp changes after passing the land-water border and in passing the water-land border as well. The main reason for these sharp changes could be related to the big difference between the water surface roughness ($z_0 = 0.0001\ m$) and the land surface ($z_0 = 0.13\ m$). Regarding the atmospheric stability conditions as shown in Table 2, in the unstable conditions, the airflow has sharp changes in passing from land through water surface or vice versa. However, for stable conditions ($t = 12:00$ and $t = 15:00\ hr$), the velocity profile has no clear pattern in the transition zones. Investigating the streamlines at these times shows that in stable conditions there are some inverse flows in the domain which could change the velocity values when compared with the effect of roughness changes. Therefore, in stable conditions (over the water surface) the effect of buoyancy on the air flow is dominant and therefore, should be considered in the ABL modeling. Including the buoyancy effect in the momentum equation could be another reason for the changes in flow parameters (Equation (2)). As shown in Table 2 at $t = 12:00\ hr$ and $t = 15:00\ hr$, the ABL is stable and the buoyancy effect could be maximum (considering the presented values in Table 2) due to the highest values of differences between the reference (T_{ref}) and air temperature (T_a). For temperature (Fig. 13(b)), its shape in streamwise ($x-$)direction in stable conditions is different from unstable conditions. In stable conditions, there are some sharp changes (either increasing or decreasing) in temperature profiles. For unstable conditions, the changes in temperature profile are small and, in general, the change

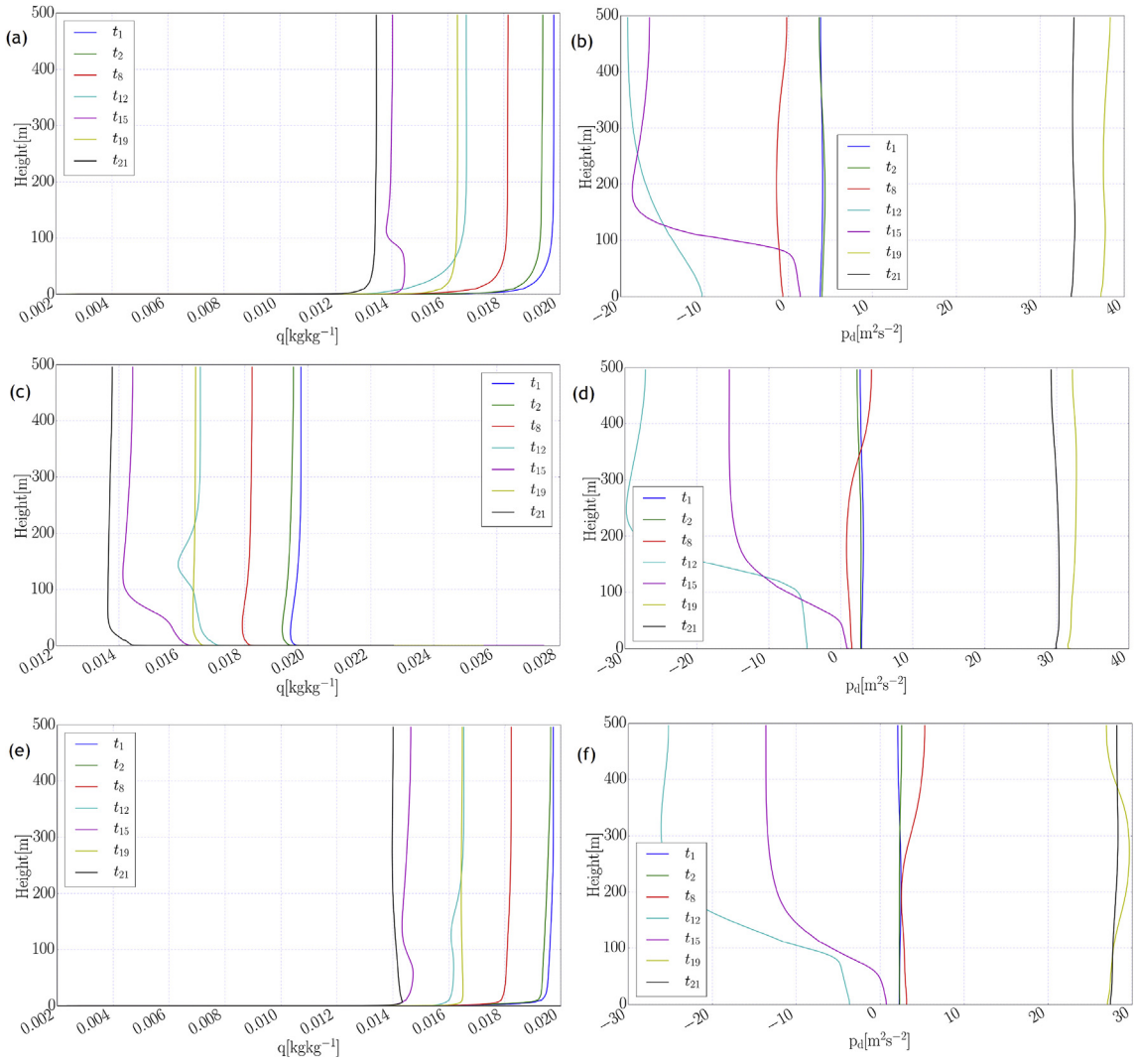

Fig. 18. Comparison of simulated flow parameters in height (z−direction) for different locations in streamwise direction and for different times: $t_1 = 01:00$, $t_2 = 02:00$, $t_8 = 08:00$, $t_{12} = 12:00$, $t_{15} = 15:00$, $t_{19} = 19:00$ and $t_{21} = 24:00\ hr$: **(a)** specific humidity at x = 500 m on land in upstream of the water surface; **(b)** dynamic pressure ($P_d = P_{total} - P_{static}$) at x = 500 m on land in upstream of the water surface; **(c)** specific humidity at x = 1000 m over the water surface; **(d)** dynamic pressure ($P_d = P_{total} - P_{static}$) at x = 1000 m over the water surface; **(e)** specific humidity at x = 1300 m on land in downstream of the water surface; **(f)** dynamic pressure ($P_d = P_{total} - P_{static}$) at x = 1300 m on land in downstream of the water surface.

in temperature due to the water surface in ABL is smaller than its effects on the velocity profile. Canvassing the airflow properties illustrated in Figs. 13 and 14 shows that the water surface generally can change the airflow parameters distribution in streamwise. These changes have different shapes in different stability conditions due to the effect of buoyancy.

To study the distribution of airflow parameters with respect to the bottom surface effects on the ABL flow, the simulated airflow parameters are depicted over the four different lines streamwise in Fig. 15 and Fig. 16 at two selected times. Two lines (x_5 and x_8) pass only from the land surface and the rest (x_6 and x_7) are located on both land and water surface. In addition, due to the transient ABL flow, the simulated results are shown in two different times ($t = 02:00$ and $t = 15:00\ hr$) where at $t = 02:00\ hr$ the ABL is unstable and in $t = 15:00\ hr$ it is stable and it could be possible to study the effect of stability conditions on the ABL flow passing through different surfaces. It is clear that the position of the water surface in the computational domain is an important parameter in the airflow in the ABL, especially in unsteady flow simulation. Examining the shape of the flow parameters (for instance q in Fig. 15(f)) shows that different locations of the water surface (for line x_6 the water surface extends from 900 to 1300 m and for the x_7 it extends from 550 to 1200 m) could generate different distributions of airflow parameters.

In Fig. 17, Fig. 18 and Fig. 19 the vertical profiles of airflow in three positions and at different times are delineated. These three positions are selected in a way that the reader is able to study the effect of water surface on the vertical profiles of airflow. The first point is located on the upstream (upwind) land before reaching the water surface ($x = 500\ m$), the second point is located on the water surface far from the water edge ($x = 1000\ m$) and the last one is located on the downstream (downwind) land after passing from the water surface ($x = 1300\ m$). As shown in these figures, the water surface makes some changes in the flow profiles not only over the water surface but also on the downwind land. It means that the combination of water surface's shape and the wind direction can significantly affect the distributions of airflow variables over the water, and in the downwind distance outside the water body itself. These effects could help in situating land-based stations to measure meteorological parameters in lake surroundings.

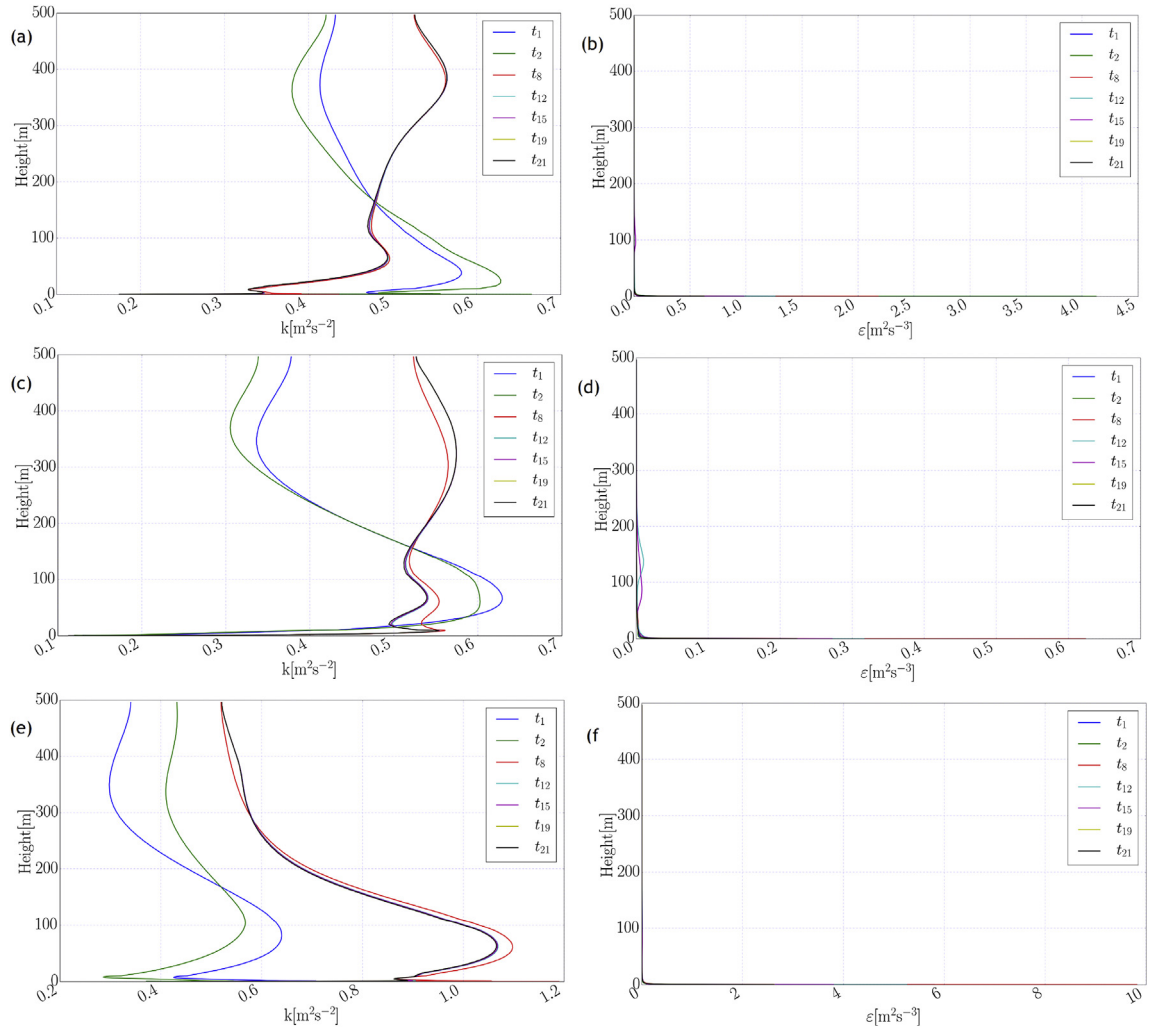

Fig. 19. Comparison of simulated flow parameters in height (z-direction) for different locations in streamwise and for different times: $t_1 = 01{:}00$, $t_2 = 02{:}00$, $t_8 = 08{:}00$, $t_{12} = 12{:}00$, $t_{15} = 15{:}00$, $t_{19} = 19{:}00$ and $t_{21} = 24{:}00$ hr: and: **(a)** turbulent kinetic energy at $x = 500\ m$ on land in upstream of the water surface; **(b)** dissipation rate of turbulent kinetic energy at $x = 500\ m$ on land in upstream of the water surface; **(c)** turbulent kinetic energy at $x = 1000\ m$ over the water surface; **(d)** dissipation rate of turbulent kinetic energy at $x = 1000\ m$ over the water surface; **(e)** turbulent kinetic energy at $x = 1300\ m$ on land in downstream of the water surface; **(f)** dissipation rate of turbulent kinetic energy at $x = 1300\ m$ on land in downstream of the water surface.

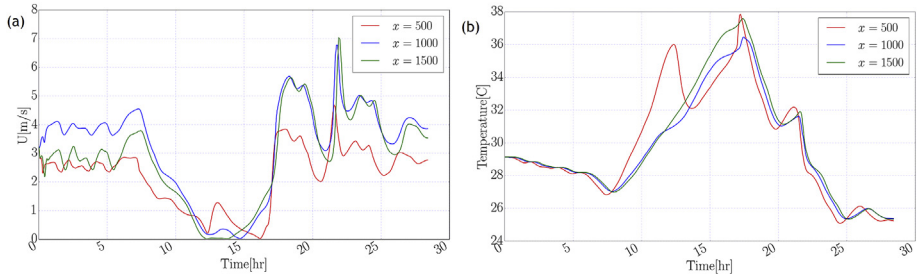

Fig. 20. Changes of simulated flow parameters with time at height of 2 m above the bottom surface in three locations: $x_1 = 500\ m$ (over the upstream land), $x_2 = 1000\ m$ (over the water surface) and $x_3 = 1500\ m$ (over the downstream land), **(a)** velocity; and **(b)** temperature.

The temporal distribution of airflow velocity, as well as the temperature distribution, are illustrated in Fig. 20(a) and Fig. 20(b) respectively. The temporal distribution are plotted for three probe locations: i) the first point is located at $x = 500$ and $z = 2.0\ m$ above the bottom surface over the upwind land, ii) the second one is at $x = 1000$ and $z = 2.0\ m$ above the water surface, and iii) the third point is located at $x = 1500$ and $z = 2.0\ m$ above the downwind land. In stable conditions ($t \approx 08:45$ till $18:00\ hr$), there is no clear trend for velocity changes in any of the selected probe locations. For unstable conditions (the remaining time), the velocity values on the water surface and on the downstream land are larger than the values on the upstream land. Fig. 20(b) shows that the changes in temperatures values for unstable conditions are very small for all locations. However, the changes in temperature increases (from

$t = 08:45\ hr$) in stable conditions, and continues until reaching unstable condition at $t = 18:00\ hr$.

The model results described above shows that the water surface can affect the airflow in ABL due to its different properties in roughness, wetness and temperature. In unstable atmospheric conditions, the water surface characteristics could change the airflow pattern when compared with a homogeneous surface (the surface which includes only land) in all directions (in streamwise, vertical and perpendicular direction). However, in stable atmospheric conditions, the airflow in ABL is affected not only by the surface characteristics but also by the atmospheric stability conditions. In these situations, there is no clear direction for parameter changes in the ABL.

8. Conclusion

In this study, the airflow in Atmospheric Boundary Layer (ABL) using Unsteady Reynolds-Averaged Navier-Stokes (URANS) is simulated considering the effects of sharp changes in surface characteristics from dry land to water surface and vice versa. In addition, the effect of atmospheric stability conditions on the airflow is examined. To be able to take into account the stability conditions and the buoyancy in the ABL and the non-homogeneity of the bottom surface as well, some modification were done in the flow equations and in the turbulence equations. Due to the complexity of the computational domain which includes an irregular water surface at the bottom surface, generating the geometry and the optimal computational grid is a big challenge for simulations. Adapting the boundary conditions to the data available and their transient conditions, need much effort to get reasonable and reliable results for the airflow in ABL. The results of the model were verified for three cases with different stability conditions. Validation results showed that the model has a good performance especially in unstable conditions.

The current model was used to investigate the effect of a small water surface on the airflow in ABL. The main reason for the simulation was to study the changes of the flow variables due to the available water surface and the effects of stability conditions on the parameters, especially over the water surface. The model was then used to determine the heat fluxes and the humidity over the water surface. The results showed that the flow pattern in the domain is affected by different parameters such as changes in roughness, wetness, temperature and the stability conditions as well. In unstable atmospheric conditions, the effect of changes in surface characteristics was dominant and a clear pattern could be detected. However, for the stable atmospheric condition no clear patterns were detected. The shape of the airflow in ABL in these conditions could be affected by the buoyancy force which is dominant compared with the changes of surface properties.

The proposed model could be used as a suitable tool to estimate parameters such as velocity, temperature, specific humidity, etc. over the water surface using measured meteorological parameters in land-based stations. In addition, the results of the model will help identify appropriate location to install weather stations on the land in lake surroundings.

Acknowledgments

This work was carried out on the Dutch national e-infrastructure with the support of SURF Foundation (under grant number e-infra140092). The work was also supported by Challenge Program on Water and Food (CPWF), the European Space Agency's TIGER project and the SOAR-Africa project by the Canadian Space Agency (CSA).

Appendix A. Software/Data Availability

In this appendix, more details about the software and tools used in this study are presented. As shown in the details, all software used are free of charge:

- **ABL-Model**
  Name of software: `ABL-Model`
  Developers: Ali Abbasi, Frank Ohene Annor and Nick van de Giesen;
  Contact address: Department of Water Resources, Faculty of Civil Engineering and Geosciences, Delft University of Technology, Stevinweg 1, 2628 CN, Delft, Netherlands;
  Email: a.abbasi@tudelft.nl & aliabbasi.civileng@gmail.com;
  Year first available: 2015
  Availability: Free and open source under the GNU General Public License (https://github.com/aabbasi59/ABL_Model);
  Dependencies: OpenFoam, swak4Foam, Python, C++;
  Cost: Free;
  Program language: C++, Python;
- **QGIS**
  Name of software: `QGIS`
  Developers: The Open Source Geospatial Foundation (OSGeo);
  Availability: Free and open source under the GNU General Public License (http://www.qgis.org/en/site/forusers/download.html);
  Cost: Free;
  Program language: Python
- **Netfabb**
  Name of software: `Netfabb Basic`
  Developers: AUTODESK;
  Availability: The Basic version is Free (https://www.netfabb.com/products/netfabb-basic);
  Cost: Free;
- **MeshLab**
  Name of software: `MeshLab`
  Developers: The Computer Science department of University of Pisa;
  Availability: Free and open source under the GNU General Public License version 2.0 (GPLv2) (https://sourceforge.net/projects/meshlab/files/latest/download);
  Cost: Free;
- **ADMESH**
  Name of software: `ADMESH`
  Availability: Free and open source under the GNU General Public License (GPL) (https://github.com/admesh/admesh);
  Cost: Free;
- **OpenFOAM**
  Name of software: `OpenFOAM`
  Developers: OpenCFD Ltd;
  Year first available: 2004;
  Availability: Free and open source under the GNU General Public License (http://www.openfoam.com/);
  Cost: Free;
  Program language: C++
- **swak4Foam**
  Name of software: `swak4Foam`
  Developers: Bernhard Gschaider;
  Email: bgschaid@ice-sf.at;
  Availability: Free and open source under the GNU General Public License (https://openfoamwiki.net/index.php/Contrib/swak4Foam);
  Cost: Free;
  Program language: Python

- **Gnuplot**
  Name of software: `Gnuplot`
  Availability: The source code is copyrighted but freely distributed (http://www.gnuplot.info/);
  Cost: Free;
- **Python**
  Program language: `Python`
  Availability: Free and open source developed under an OSI-approved open source license (https://www.python.org/);
  Cost: Free;

References

Abbasi, A., Annor, F.O., van de Giesen, N., 2016. Investigation of temperature dynamics in small and shallow reservoirs. Case study: lake Binaba, Upper East region of Ghana. Water 8, 84.

Abbasi, A., Annor, F.O., van de Giesen, N., 2017a. A framework to simulate small shallow inland water bodies in semi-arid regions. Adv. Water Resour. 110 (Suppl. C), 77–96. http://www.sciencedirect.com/science/article/pii/S0309170816302238.

Abbasi, A., Annor, F.O., van de Giesen, N., 2017b. Developing a CFD-based approach to estimate evaporation from water surfaces in (Semi-)Arid regions. Hydrological Processes (Manuscript submitted for publication).

Abbasi, A., Annor, F.O., van de Giesen, N., 2017c. Effects of atmospheric stability conditions on heat fluxes from small water surfaces in (semi-)Arid regions. Hydrol. Sci. J. 9 (62), 1422–1439. https://doi.org/10.1080/02626667.2017.1329587.

Albertson, J., Parlange, M.B., nov 1999. Natural integration of scalar Fuxes from complex terrain. Adv. Water Resour. 23 (3), 239–252. http://linkinghub.elsevier.com/retrieve/pii/S0309170899000111.

Alinot, C., Masson, C., 2005. k- model for the atmospheric boundary layer under various thermal stratifications. J. Sol. Energy Eng. 127, 438–443.

Anagnostopoulos, J., Bergeles, G., mar 1998. A numerical model for wind field and pollutant concentration calculations over complex terrain. Application to Athens, Greece. J. Wind Eng. Ind. Aerod. 73, 285–306.

Annor, F., van de Giesen, N., Liebe, J., van de Zaag, P., Tilmant, A., Odai, S., 2009. Delineation of small reservoirs using radar imagery in a semi-arid environment: a case study in the upper east region of Ghana. Phys. Chem. Earth 34 (4–5), 309–315.

Avissar, R., Pielke, R.a, 1989. A Parameterization of Heterogeneous Land Surfaces for Atmospheric Numerical Models and its Impact on Regional Meteorology.

Bagayoko, F., Yonkeu, S., Elbers, J., van de Giesen, N., feb 2007. Energy partitioning over the West African savanna: multi-year evaporation and surface conductance measurements in Eastern Burkina Faso. J. Hydrol. 334, 545–559.

Balogh, M., Parente, A., Benocci, C., mar 2012. RANS simulation of ABL flow over complex terrains applying an Enhanced k-ε model and wall function formulation: implementation and comparison for fluent and OpenFOAM. J. Wind Eng. Ind. Aerod. 104–106, 360–368.

Bechmann, A., 2006. Large-eddy Simulation of Atmospheric Flow over Complex Terrain. Phd thesis. Technical University of Denmark.

Beniston, M., 1986. The influence of a water surface on mesoscale dynamics as a function of atmospheric stability. Boundary-Layer Meteorol. 36, 19–37.

Benjamin, C., Bogdan, T., Daniele, C., 2011. Hybrid assessment method for LES models. In: Kuerten, H., Geurts, B., Armenio, V., Fröhlich, J. (Eds.), Direct and Large-eddy Simulation VIII. Vol. 15 of ERCOFTAC Series. Springer Netherlands, Dordrecht, pp. 33–38.

Benjamin Martinez, 2011. Wind Resource in Complex Terrain with OpenFOAM. Master thesis, National Laboratory for Sustainable Energy. Technical University of Denmark.

Beyers, M., Jackson, D., Lynch, K., Cooper, A., Baasd, A., Delgado-Fernandezb, I., Dallairea, P.-O., 2010. Field testing and CFD LES simulation of offshore wind flows over coastal dune terrain in Northern Ireland. In: CWE2010, pp. 1–8.

Blocken, B., Stathopoulos, T., Carmeliet, J., jan 2007. CFD simulation of the atmospheric boundary layer: wall function problems. Atmos. Environ. 41, 238–252.

Bou-Zeid, E., 2004. Large-eddy simulation of neutral atmospheric boundary layer flow over heterogeneous surfaces: blending height and effective surface roughness. Water Resour. Res. 40 (2), 1–18. http://www.agu.org/pubs/crossref/2004/2003WR002475.shtml.

Bou-Zeid, E., Meneveau, C., Parlange, M.B., 2004. Large-eddy simulation of neutral atmospheric boundary layer flow over heterogeneous surfaces: blending height and effective surface roughness. Water Resour. Res. 40, 1–18. http://www.agu.org/pubs/crossref/2004/2003WR002475.shtml.

Bradley, E.F., 1968. A micrometeorological study of velocity profiles and surface drag in the region modified by a change in surface roughness. Q. J. Roy. Meteorol. Soc. 94 (401), 361–379. http://onlinelibrary.wiley.com/doi/10.1002/qj.49709440111/abstract.

Brockhaus, G.T., 2011. Hydrodynamic Design of Ship Bulbous Bows Considering Seaway and Operational Conditions. Phd thesis. Technischen Universit at Berlin.

Brutsaert, W., 1982. Evaporation into the Atmosphere: Theory, History, and Applications. Reidel, Dordrecht.

Cabot, W., Moin, P., 1999. Approximate wall boundary conditions in the large-eddy simulation of high Reynolds number flow. Flow, Turbul. Combust. 63, 269–291.

Cancelli, D.M., Chamecki, M., Dias, N.L., jan 2014. A large-eddy simulation study of scalar dissimilarity in the convective atmospheric boundary layer. J. Atmos. Sci. 71 (1), 3–15. http://journals.ametsoc.org/doi/abs/10.1175/JAS-D-13-0113.1.

Cao, S., Tamura, T., jan 2006. Experimental study on roughness effects on turbulent boundary layer flow over a two-dimensional steep hill. J. Wind Eng. Ind. Aerod. 94, 1–19.

Cebeci, T., 2004. Analysis of Turbulent Flows. Elsevier, Oxford.

Chamecki, M., Meneveau, C., Parlange, M.B., aug 2008. A hybrid spectral/finite-volume algorithm for large-eddy simulation of scalars in the atmospheric boundary layer. Boundary-Layer Meteorol. 128 (3), 473–484.

Chen, G., Xiong, Q., Morris, P.J., Paterson, E.G., Sergeev, A., Wang, Y.-C., apr 2014. OpenFOAM for computational Fluid dynamics. Not. AMS 61 (4), 354. http://www.ams.org/jourcgi/jour-getitem?pii=noti1095.

Churchfield, M.J., 2013. Adding Complex Terrain and Stable Atmospheric Condition Capability to the Simulator for On/Offshore Wind Farm Applications (SOWFA).

Collaborative Organisation for ICT in Dutch Higher Education and Research, 2017. SURFsara[online]. Available from: https://www.surf.nl/en/services-and-products/hpc-cloud/technical-specifications/index.html, [Accessed 25 September 2017].

Corzo, S.F., Damián, S.M., Ramajo, D., Norberto, M.N., 2011. Numerical simulation of natural convection phenomena. Mecánica Computacional XXX, 277–296.

Crasto, G., 2007. Numerical simulations of the atmospheric boundary layer. Phd thesis. Università degli Studi di Cagliari.

Crosman, E.T., Horel, J.D., jun 2010. Sea and lake breezes: a review of numerical studies. Boundary-Layer Meteorol. 137, 1–29.

Davenport, D.C., Hudson, J.P., 1967. Changes in evaporation rates along a 17-KM transect in the Sudan Gezira. Agric. Meteorol. 4, 339–352.

DeCosmo, J., Katsaros, K.B., Smith, S.D., Anderson, R.J., Oost, W.a., Bumke, K., Chadwick, H., 1996. Air-sea exchange of water vapor and sensible heat: the Humidity Exchange over the Sea (HEXOS) results. J. Geophys. Res. 101, 12001.

Defraeye, T., Blocken, B., Carmeliet, J., sep 2012. Analysis of convective heat and mass transfer coefficients for convective drying of a porous flat plate by conjugate modelling. Int. J. Heat Mass Tran. 55, 112–124. http://linkinghub.elsevier.com/retrieve/pii/S0017931011004923.

Dyer, A.J., Crawford, T.V., 1965. Observations of the modification of the microclimate at a leading edge. Q. J. Roy. Meteorol. Soc. 91, 345–348. http://doi.wiley.com/10.1002/qj.49709138909.

Edson, J., Crawford, T., Crescenti, J., Farrar, T., Frew, N., Gerbi, G., Plueddemann, A., Trowbridge, J., Weller, R., Williams, A.J., Helmis, C., Hristov, T., Shen, L., Khelif, D., Jessup, A., Jonsson, H., Li, M., Mahrt, L., Skyllingstad, E., Vickers, D., McGillis, W., Zappa, C., Stanton, T., Wang, Q., Sullivan, P., Sun, J., Wang, S., Wilkin, J., Yue, D.K.P., mar 2007. The coupled boundary layers and air-sea transfer experiment in low winds. Bull. Am. Meteorol. Soc. 88, 341–356. http://journals.ametsoc.org/doi/abs/10.1175/BAMS-88-3-341.

Esau, I.N., Lyons, T.J., 2002. Effect of sharp vegetation boundary on the convective atmospheric boundary layer. Agric. For. Meteorol. 114, 3–13.

Ferziger, J.H., Perić, M., 2002. Computational Methods for Fluid Dynamics, third ed. Springer-Verlag.

Fesquet, C., Drobinski, P., Barthlott, C., Dubos, T., oct 2009. Impact of terrain heterogeneity on near-surface turbulence structure. Atmos. Res. 94, 254–269. http://linkinghub.elsevier.com/retrieve/pii/S0169809509001665.

Figuerola, P.I., Berliner, P.R., 2005. Evapotranspiration under advective conditions. Int. J. Biometeorol. 49, 403–416.

Flores, F., Garreaud, R., Muñoz, R.C., aug 2013. CFD simulations of turbulent buoyant atmospheric flows over complex geometry: solver development in OpenFOAM. Comput. Fluid 82, 1–13. http://linkinghub.elsevier.com/retrieve/pii/S0045793013001795.

Fluent Manual, 2006. Natural Convection and Buoyancy-driven Flows.

Foudhil, H., Brunet, Y., Caltagirone, J.P., jun 2005. A fine-scale k-ε model for atmospheric flow over heterogeneous landscapes. Environ. Fluid Mech. 5, 247–265. http://www.springerlink.com/index/10.1007/s10652-004-2124-x.

Fredriksson, S., 2011. A BuoyantBoussinesqSurfactantFoam Tutorial- an Introduction to FAM. Tech. rep. Chalmers University of Technology.

Gao, Y., Chen, F., Barlage, M., Liu, W., Cheng, G., Li, X., Yu, Y., Ran, Y., Li, H., Peng, H., Ma, M., 2008. Enhancement of land surface information and its impact on atmospheric modeling in the Heihe River Basin, northwest China. J. Geophys. Res. 113, 1–19.

Garratt, J., oct 1994. Review: the atmospheric boundary layer. Earth Sci. Rev. 37 (1–2), 89–134. http://linkinghub.elsevier.com/retrieve/pii/0012825294900264.

Giorgi, F., Avissar, R., 1997. Representation of heterogeneity effects in Earth system modeling: experience from land surface modeling. Rev. Geophys. 35 (97), 413.

Hargreaves, D., Wright, N., may 2007. On the use of the k-ε model in commercial CFD software to model the neutral atmospheric boundary layer. J. Wind Eng. Ind. Aerod. 95, 355–369. http://linkinghub.elsevier.com/retrieve/pii/S016761050600136X.

Heikinheimo, M., Kangas, M., Tourula, T., Vena, A., Tattari, S., 1999. Momentum and heat fluxes over lakes Tamnaren and Raksjo determined by the bulk-aerodynamic and eddy-correlation methods. Agric. For. Meteorol. 89–99, 521–534.

Hertwig, D., Leitl, B., Schatzmann, M., apr 2011. Organized turbulent structuresLink between experimental data and LES. J. Wind Eng. Ind. Aerod. 99, 296–307. http://linkinghub.elsevier.com/retrieve/pii/S0167610511000043.

Hsieh, K.-J., Lien, F.-S., Yee, E., dec 2007. Numerical modeling of passive scalar

dispersion in an urban canopy layer. J. Wind Eng. Ind. Aerod. 95, 1611–1636. http://linkinghub.elsevier.com/retrieve/pii/S0167610507000761.
Huser, A., Nilsen, P.J., Skatun, H., 1997. Application of k-ε model to the stable ABL: pollution in complex terrain. J. Wind Eng. Ind. Aerod. 67 & 68, 425–436. http://www.sciencedirect.com/science/article/pii/S0167610597000913.
Hussein, A.S., El-Shishiny, H., mar 2009. Influences of wind flow over heritage sites: a case study of the wind environment over the Giza Plateau in Egypt. Environ. Model. Software 24 (3), 389–410. http://linkinghub.elsevier.com/retrieve/pii/S1364815208001497.
Jackson, N.A., 1976. The propagation of modified flow downstream of a change in surface roughness. Q. J. Roy. Meteorol. Soc. 102, 924–933.
Joubert, E.C., Harms, T.M., Muller, A., Hipondoka, M., Henschel, J.R., 2012. A CFD study of wind patterns over a desert dune and the effect on seed dispersion. Environ. Fluid Mech. 12, 23–44.
Józsa, J., Milici, B., Napoli, E., nov 2007. Numerical simulation of internal boundary-layer development and comparison with atmospheric data. Boundary-Layer Meteorol. 123, 159–175. http://www.springerlink.com/index/10.1007/s10546-006-9134-9.
Keller, A., Sakthivadivel, R., Seckler, D., 2000. Water Scarcity and the Role of Storage in Development. Tech. rep., Technical Report. International Water Management Institute, International Water Management Institute, Colombo.
Kim, H., Lee, C., Lim, H., Kyong, N., 1997. An experimental and numerical study on the flow over two-dimensional hills. J. Wind Eng. Ind. Aerod. 66, 17–33. http://www.sciencedirect.com/science/article/pii/S016761059700007X.
Kim, H., Patel, V., Lee, C., 2000. Numerical simulation of wind flow over hilly terrain. J. Wind Eng. Ind. Aerod. 87, 45–60. http://www.sciencedirect.com/science/article/pii/S0167610500000143.
Kim, H.G., Patel, V.C., 2000. Test of turbulence models for wind flow over terrain with separatin and recirculation. Boundary-Layer Meteorol. 94, 5–21.
Kim, S.-E., Boysan, F., 1999. Application of CFD to environmental flows. J. Wind Eng. Ind. Aerod. 81 (1–3), 145–158.
Koblitz, T., Bechmann, A., Sogachev, A., Sørensen, N., Réthoré, P.E., 2015. Computational Fluid Dynamics model of stratified atmospheric boundary-layer flown. Wind Energy 18, 75–89.
Lang, A.R.G., Evans, G.N., Ho, P.Y., 1974. The influence of local advection on evapotranspiration from irrigated rice in a semi-arid region. Agric. Meteorol. 13, 5–13.
Lang, A.R.G., McNaughton, K.G., Fazu, C., Bradely, E.F., Ohtaki, E., 1983. An experimental appraisal of the terms in the heat and moisture flux equations for local advection. Boundary-Layer Meteorol. 25, 89–102.
Lee, J.W., 2007. Numerical Modelling of Temperature-induced Circulation in Shallow Water Bodies and Application to Torrens Lake, South Australia. Doctoral thesis, PhD Thesis. The University of Adelaide Applied Mathematics. http://digital.library.adelaide.edu.au/dspace/handle/2440/37895.
Lettau, H., Zabransky, J., 1968. Interrelated changes of wind profile structure and richardson number in air flow from land to inland lakes. J. Atmos. Sci. 25, 718–728. http://adsabs.harvard.edu/abs/1968JAtS...25..718L.
Liu, J., Chen, J.M., Black, T.A., Novak, M.D., 1996. E-epsilon modelling of turbulent air flow downwind of a model forest edge. Boundary-Layer Meteorol. 77, 21–44.
Luna, Y.F., Mochidaa, A., Murakamib, S., Yoshinoa, H., Shirasawa, T., 2003. Numerical simulation of flow over topographic features by revised k-epsilon models. J. Wind Eng. Ind. Aerod. 91, 231–245.
Lyons, T.J., Halldin, S., 2004. Surface heterogeneity and the spatial variation of fluxes. Agric. For. Meteorol. 121, 153–165.
Mahrt, L., MacPherson, J., Desjardins, R., 1994. Observations of fluxes over heterogeneous surfaces. Boundary-Layer Meteorol. 67, 345–367.
Majdoubi, H., Boulard, T., Fatnassi, H., Bouirden, L., jun 2009. Airflow and microclimate patterns in a one-hectare Canary type greenhouse: an experimental and CFD assisted study. Agric. For. Meteorol. 149 (6–7), 1050–1062. http://linkinghub.elsevier.com/retrieve/pii/S0168192309000045.
Maronga, B., Moene, A.F., van Dinther, D., Raasch, S., Bosveld, F.C., Gioli, B., 2013. Derivation of structure parameters of temperature and humidity in the convective boundary layer from large-eddy simulations and implications for the interpretation. Boundary-Layer Meteorol. 1–30. http://link.springer.com/article/10.1007/s10546-013-9801-6.
Massel, S.R., 1999. Fluid Mechanics for Marine Ecologists. Springer Berlin Heidelberg.
Meissner, C., Gravdahl, A.R., Steensen, B., 2009. Including thermal effects in CFD wind flow simulations. J. Environ. Sci. 18 (8), 833–839.
Milashuk, S., Crane, W.A., apr 2011. Wind speed prediction accuracy and expected errors of RANS equations in low relief inland terrain for wind resource assessment purposes. Environ. Model. Software 26 (4), 429–433. http://linkinghub.elsevier.com/retrieve/pii/S136481521000263X.
Munro, D.S., Oke, T.R., 1975. Aerodynamic boundary-layer adjustment over a crop in neutral stability. Boundary-Layer Meteorol. 9, 53–61. http://www.springerlink.com/index/g830n417574u719l.pdf.
Nadeau, D.F., Pardyjak, E.R., Higgins, C.W., Fernando, H.J.S., Parlange, M.B., aug 2011. A simple model for the afternoon and early evening decay of convective turbulence over different land surfaces. Boundary-Layer Meteorol. 141 (2), 301–324. http://www.springerlink.com/index/10.1007/s10546-011-9645-x.
OSullivan, J., Archer, R., Flay, R., jan 2011. Consistent boundary conditions for flows within the atmospheric boundary layer. J. Wind Eng. Ind. Aerod. 99 (1), 65–77. http://linkinghub.elsevier.com/retrieve/pii/S0167610510001182.
Panofsky, H.A., Petersen, E.L., 1972. Wind profiles and change of terrain roughness at Riso. Q. J. Roy. Meteorol. Soc. 98, 845–854.
Panofsky, H.A., Townsend, A.A., 1964. Change of terrain roughness and the wind profile. Q. J. Roy. Meteorol. Soc. 90, 147–155.
Parente, A., Gorlé, C., van Beeck, J., Benocci, C., apr 2011. Improved k-epsilon model and wall function formulation for the RANS simulation of ABL flows. J. Wind Eng. Ind. Aerod. 99, 267–278. http://linkinghub.elsevier.com/retrieve/pii/S016761051100002X.
Parlange, M.B., Eichinger, W.E., Albertson, J.D., 1995. Regional scale evaporation and the atmospheric boundary layer. Rev. Geophys. 33 (1), 99–124. http://onlinelibrary.wiley.com/doi/10.1029/94RG03112/full.
Pattanapol, W., Wakes, S.J., Hilton, M.J., Dickinson, K.J., 2008. Modeling of surface roughness for flow over a complex vegetated surface. International Journal of Engineering and Natural Sciences 2 (1), 18–26.
Pendergrass, W., Arya, S., jan 1984. Dispersion in neutral boundary layer over a step change in surface roughness-I. Mean flow and turbulence structure. Atmos. Environ. 18 (7), 1267–1279. http://linkinghub.elsevier.com/retrieve/pii/0004698184900374.
Petersen, E.L., Taylor, P.A., 1973. Some comparisons between observed wind profiles at Riso and theoretical predictions for flow over inhomogeneous terrain. Q. J. Roy. Meteorol. Soc. 99, 329–336.
Pielke, R.a., Uliasz, M., 1998. Use of meteorological models as input to regional and mesoscale air quality models - limitations and strengths. Atmos. Environ. 32 (8), 1455–1466.
Pieterse, J.E., 2013. CFD Investigation of the Atmospheric Boundary Layer under Different Thermal Stability Conditions. Ph.D. thesis. Stellenbosch University.
Piomelli, U., aug 2008. Wall-layer models for large-eddy simulations. Prog. Aero. Sci. 44, 437–446. http://linkinghub.elsevier.com/retrieve/pii/S037604210800047X.
Piomelli, U., Balaras, E., 2002. Wall-layer models for large-eddy simulations. Annu. Rev. Fluid Mech. 34, 349–374. http://www.annualreviews.org/doi/pdf/10.1146/annurev.fluid.34.082901.144919.
Pontiggia, M., Derudi, M., Busini, V., Rota, R., nov 2009. Hazardous gas dispersion: a CFD model accounting for atmospheric stability classes. J. Hazard Mater. 171, 739–747. http://www.ncbi.nlm.nih.gov/pubmed/19619939.
Porté-Agel, F., Lu, H., Wu, Y.-T., 2014. Interaction between large wind farms and the atmospheric boundary layer. In: Procedia IUTAM. Vol. 10. Elsevier B.V., pp. 307–318. http://linkinghub.elsevier.com/retrieve/pii/S2210983814000273
Porté-Agel, F., Wu, Y.-T., Lu, H., Conzemius, R.J., apr 2011. Large-eddy simulation of atmospheric boundary layer flow through wind turbines and wind farms. J. Wind Eng. Ind. Aerod. 99, 154–168. http://linkinghub.elsevier.com/retrieve/pii/S0167610511000134.
Prospathopoulos, J., Politis, E., Chaviaropoulos, P., aug 2012. Application of a 3D RANS solver on the complex hill of Bolund and assessment of the wind flow predictions. J. Wind Eng. Ind. Aerod. 107–108, 149–159. http://linkinghub.elsevier.com/retrieve/pii/S0167610512001134.
Prospathopoulos, J., Voutsinas, S.G., 2006. Implementation issues in 3D wind flow predictions over complex terrain. J. Sol. Energy Eng. 128, 539.
Raupach, M.R., Finnigan, J.J., Brunei, Y., mar 1996. Coherent eddies and turbulence in vegetation canopies: the mixing-layer analogy. Boundary-Layer Meteorol. 78 (3–4), 351–382. http://www.springerlink.com/index/10.1007/BF00120941.
Raupach, M.R., Thom, A.S., Edwards, I., 1980. A wind-tunnel study of turbulent flow close to regularly arrayed rough surfaces. Boundary-Layer Meteorol. 18, 373–397.
Rhoads, J., 2014. Effects of Grid Quality on Solution Accuracy. Tech. rep.
Rider, N.E., Philip, J.R., Bradley, E.F., 1964. The horizontal transport of heat and moisture- a micrometeorological study. Q. J. Roy. Meteorol. Soc. 84, 507–530. http://onlinelibrary.wiley.com/doi/10.1002/qj.49708938207/abstract.
Rohdin, P., Moshfegh, B., 2007. Numerical predictions of indoor climate in large industrial premises. A comparison between different k-ε models supported by field measurements. Build. Environ. 42, 3872–3882.
Shih, T.-H., Liou, W.W., Shabbir, A., Yang, Z., Zhu, J., 1995. A new k-ε eddy viscosity model for high Reynolds number turbulent flows. Comput. Fluid 24 (3), 227–238.
Silvester, S.a., Lowndes, I.S., Hargreaves, D.M., 2009. A computational study of particulate emissions from an open pit quarry under neutral atmospheric conditions. Atmos. Environ. 43 (40), 6415–6424. https://doi.org/10.1016/j.atmosenv.2009.07.006.
Sogachev, A., Kelly, M., Leclerc, M.Y., 2012. Consistent two-equation closure modelling for atmospheric research: buoyancy and vegetation implementations. Boundary-Layer Meteorol. 145, 307–327.
Solazzo, E., Cai, X., Vardoulakis, S., 2009. Improved parameterisation for the numerical modelling of air pollution within an urban street canyon. Environ. Model. Software 24 (3), 381–388. https://doi.org/10.1016/j.envsoft.2008.08.001.
Sun, J., Vandemark, D., Mahrt, L., Vickers, D., Crawford, T., Vogel, C., 2001. Momentum transfer over the coastal zone. J. Geophys. Res. 106, 12437–14248.
Swayne, D., Lam, D., Mackay, M., Rouse, W., Schertzer, W., dec 2005. Assessment of the interaction between the canadian regional climate model and lake thermalhydrodynamic models. Environ. Model. Software 20 (12), 1505–1513. http://linkinghub.elsevier.com/retrieve/pii/S1364815205001027.
Tritton, D., 2007. Physical Fluid Dynamics. Oxford Science Publications.
Tsanis, I.K., Wu, J., Shen, H., Valeo, C., 2006. Environmental hydraulics: hydrodynamic and pollutant transport modelling of lakes and coastal waters. In: Tsanis, I.K., Wu, Jian, S, H., Valeo, C. (Eds.), Book. Developments in Water Science. Elsevier. http://www.sciencedirect.com/science/article/pii/S0167564806560010.
Vendel, F., Lamaison, G., Soulhac, L., Volta, P., Donnat, L., Duclaux, O., Puel, C., 2010. Modelling diabatic atmospheric boundary layer using a RANS CFD code with a k-ε turbulence closure. In: HARMO13. Vol. 0, pp. 652–656.

Vercauteren, N., 2011. Water Vapor and Heat Exchange over Lakes. Phd thesis. École Polytechnique Fééérale de Lausanne.

Vercauteren, N., Bou-Zeid, E., Parlange, M.B., Lemmin, U., Huwald, H., Selker, J., Meneveau, C., jul 2008. Subgrid-scale dynamics of water vapour, heat, and momentum over a lake. Boundary-Layer Meteorol. 128 (2), 205–228. http://www.springerlink.com/index/10.1007/s10546-008-9287-9.

Verdier-Bonnet, C., Angot, P., Fraunie, P., Coantic, M., jun 1999. Three-dimensional modelling of coastal circulations with different k-ϵ closures. J. Mar. Syst. 21, 321–339. http://linkinghub.elsevier.com/retrieve/pii/S0924796399000214.

Vickers, D., Mahrt, L., apr 2010. Sea-surface roughness lengths in the midlatitude coastal zone. Q. J. Roy. Meteorol. Soc. 136 (649), 1089–1093. http://doi.wiley.com/10.1002/qj.617.

Vinnichenko, N.A., Uvarov, A.V., Plaksina, Y.Y., Vetukov, D.A., 2011. Study of evaporation from water reservoir. In: 22nd International Symposium on Transport Phenomena. Delft, Netherlands, pp. 1–11.

Wakes, S.J., Maegli, T., Dickinson, K.J., Hilton, M.J., 2010. Numerical modelling of wind flow over a complex topography. Environ. Model. Software 25, 237–247. http://linkinghub.elsevier.com/retrieve/pii/S136481520900200X.

Wang, Y., 2013. Development of a numerical tool to predict hydrodynamics, temperature and TDG. In: Hydropower Flows. Phd thesis. University of Iowa.

White, F.M., 1991. Viscous Fluid Flow, second ed. McGraw-Hill, New York.

Wu, Y., Nair, U.S., Pielke, R.a, McNider, R.T., Christopher, S. a., Anantharaj, V.G., 2009. Impact of land surface heterogeneity on mesoscale atmospheric dispersion. Boundary-Layer Meteorol. 133, 367–389.

Yang, Y., Gu, M., Chen, S., Jin, X., feb 2009. New inflow boundary conditions for modelling the neutral equilibrium atmospheric boundary layer in computational wind engineering. J. Wind Eng. Ind. Aerod. 97, 88–95. http://linkinghub.elsevier.com/retrieve/pii/S0167610508001815.

Zhang, A., Gao, C., Zhang, L., 2005. Numerical simulation of the wind field around different building arrangements. J. Wind Eng. Ind. Aerod. 93, 891–904.